ANNUAL REVIEWS

Annual Review of Nuclear and Particle Science

The CKM Parameters

Sébastien Descotes-Genon[1] and Patrick Koppenburg[2]

[1]Laboratoire de Physique Théorique (UMR 8627), CNRS, Université Paris-Sud and Université Paris-Saclay, 91405 Orsay, France; email: sebastien.descotes-genon@th.u-psud.fr

[2]Nikhef, 1098 XG Amsterdam, Netherlands; email: patrick.koppenburg@nikhef.nl

Annu. Rev. Nucl. Part. Sci. 2017. 67:97–127

First published as a Review in Advance on August 7, 2017

The *Annual Review of Nuclear and Particle Science* is online at nucl.annualreviews.org

https://doi.org/10.1146/annurev-nucl-101916-123109

Keywords

CKM matrix, flavor physics, Standard Model, beyond the Standard Model, *CP* violation, global fits

Abstract

The Cabibbo–Kobayashi–Maskawa (CKM) matrix is a key element in describing flavor dynamics in the Standard Model. With only four parameters, this matrix is able to describe a large range of phenomena in the quark sector, such as *CP* violation and rare decays. It can thus be constrained by many different processes, which have to be measured experimentally with high accuracy and computed with good theoretical control. Recently, with the advent of the *B* factories and the LHCb experiment taking data, the precision has significantly improved. We review the most relevant experimental constraints and theoretical inputs and present fits to the CKM matrix for the Standard Model and for some topical model-independent studies of New Physics.

Contents

1. INTRODUCTION

The study of elementary particles and their electromagnetic, weak and strong interactions has led to a particularly successful theory, the Standard Model (SM). The SM has been extensively tested, culminating with the recent discovery of the Higgs boson (1, 2) at the Large Hadron Collider (LHC). In the development of this description, quark flavor physics has played a central role in two different aspects. First, the SM embeds the Kobayashi–Maskawa mechanism: The Cabibbo–Kobayashi–Maskawa (CKM) mixing matrix (3, 4) arising in charged weak interactions represents the single source of all observed differences between particles and antiparticles, namely *CP* violation in the quark sector. Second, flavor-changing currents (in particular, neutral ones) have repeatedly revealed evidence for new, heavier degrees of freedom (charm quark, weak gauge bosons, top quark) before their discovery.

Yet the SM fails in some key aspects. Why is there such a large number of parameters for quark masses and the CKM mixing matrix, spanning such a wide range of values? Why are the electroweak and strong interactions treated separately? Why is antimatter absent from the observed universe, even though the amount of *CP* violation in the SM is too small to produce the observed matter–antimatter asymmetry (5–8)? New Physics (NP) extensions of the SM are expected to address these issues by including heavier particles related to higher-energy phenomena. The related shorter-distance interactions would have immediate consequences not only in production experiments at high energies but also through deviations from the SM predictions in flavor processes (new sources of *CP* violation, interferences between SM and NP contributions).

Therefore, a precision study of the CKM matrix is certainly desirable from a practitioner's point of view: Performing the metrology of the SM parameters yields accurate predictions for weak transitions, including *CP*-violating processes. But it is also required from a more theoretical point of view: The mixing due to the CKM matrix in weak processes has a very simple and constrained structure in the SM and is generally affected significantly by NP extensions, constituting a very powerful probe of models beyond the SM. The need for an accurate determination of the CKM matrix has led to an impressive effort from the experimental community, specifically the extensive research performed at the BaBar and Belle experiments, the large data samples available at the LHC, and the advent of the high-luminosity Belle-II B factory. The theoretical community has also made remarkable progress in the understanding of strong and weak interactions of the quarks, both analytically (in particular, through the development of effective theories) and numerically (with improvements in lattice simulations of QCD). Thus, very high precision measurements of CKM parameters are both needed and currently accessible, and they are the object of this review. We discuss the theoretical grounds related to the CKM matrix in Section 2, review the main experimental constraints on its parameters in Section 3, and present examples of global analyses of the CKM matrix and the impact of NP contributions in Section 4.

2. THE CKM MATRIX

2.1. Structure of the CKM Matrix

In the SM, the Lagrangian for the Yukawa coupling of the Higgs boson to the quark fields yields (after electroweak symmetry breaking)

$$\mathcal{L}_M^q = -(M_d)_{ij}\overline{D'_{Li}}D'_{Rj} - (M_u)_{ij}\overline{U'_{Li}}U'_{Rj}, \qquad 1.$$

where i and j are family indices, with $U' = (u', c', t')$ and $D = (d', s', b')$, and L and R indicate the components with left- and right-handed chiralities, respectively. The prime symbols indicate that these fields are not necessarily the mass eigenstates of the theory. The matrices M_u and M_d are related to the Yukawa coupling matrices as $M_q = vY^q/\sqrt{2}$, where v is the vacuum expectation value (the neutral component) of the Higgs field. At this stage, M_u and M_d are general complex matrices to be diagonalized using the singular value decomposition $M_q = V^\dagger_{qL} m_q V_{qR}$, where $V_{L,R}$ is unitary and m_q is diagonal, real, and positive. The mass eigenstates are identified as $U_L = V_{uL}U'_L$ and $U_R = V_{uR}U'_R$, and similarly for D.

Expressing the interactions of quarks with gauge bosons in terms of mass eigenstates does not modify the structure of the Lagrangian in the case of neutral gauge bosons, but it affects charged-current interactions between quarks and $W^\pm$, described by the Lagrangian

$$\mathcal{L}_{W^\pm} = -\frac{g}{\sqrt{2}}\overline{U}_i\gamma^\mu\frac{1-\gamma^5}{2}(V_{\text{CKM}})_{ij}\,D_j W^+_\mu + \text{h.c.}, \qquad 2.$$

where g is the electroweak coupling constant and $V_{\text{CKM}} = V^\dagger_{uL}V_{dL}$ is the unitary CKM matrix:

$$V_{\text{CKM}} = \begin{pmatrix} V_{ud} & V_{us} & V_{ub} \\ V_{cd} & V_{cs} & V_{cb} \\ V_{td} & V_{ts} & V_{tb} \end{pmatrix}. \qquad 3.$$

The CKM matrix induces flavor-changing transitions inside and between generations in the charged sector at tree level ($W^\pm$ interaction). By contrast, there are no flavor-changing transitions in the neutral sector at tree level (Z^0 and photon interactions). The CKM matrix stems from the Yukawa interaction between the Higgs boson and the fermions, and it originates from the misalignment in flavor space of the up and down components of the $SU(2)_{\text{L}}$ quark doublets of the SM (as there is no dynamical mechanism in the SM to enforce $V_{uL} = V_{dL}$). The $V_{\text{CKM},ij}$ CKM matrix elements (hereafter, V_{ij}) represent the couplings between up-type quarks $U_i = (u, c, t)$ and down-type quarks $D_j = (d, s, b)$. There is some arbitrariness in the conventions used to define this matrix. In particular, the relative phases among the left-handed quark fields can be redefined, reducing the number of real parameters describing this unitary matrix from three moduli and six phases to three moduli and one phase [more generally, for N generations, one has $N(N-1)/2$ moduli and $(N-1)(N-2)/2$ phases]. Because CP conjugate processes correspond to interaction terms in the Lagrangian related by Hermitian conjugation, the presence of a phase, and thus the complex nature of the CKM matrix, may induce differences between rates of CP conjugate processes, leading to CP violation. This does not occur for only two generations, where V_{CKM} is real and parameterized by a single real parameter, the Cabibbo angle.

According to experimental evidence, transitions within the same generation are characterized by V_{CKM} elements of $\mathcal{O}(1)$. Those between the first and second generations are suppressed by a factor of $\mathcal{O}(10^{-1})$; those between the second and third generations by a factor of $\mathcal{O}(10^{-2})$; and those between the first and third generations by a factor of $\mathcal{O}(10^{-3})$. This hierarchy can be expressed by defining the four phase convention–independent quantities as follows:

$$\lambda^2 = \frac{|V_{us}|^2}{|V_{ud}|^2+|V_{us}|^2}, \qquad A^2\lambda^4 = \frac{|V_{cb}|^2}{|V_{ud}|^2+|V_{us}|^2}, \qquad \bar\rho + i\bar\eta = -\frac{V_{ud}V_{ub}^*}{V_{cd}V_{cb}^*}. \tag{4}$$

An alternative convention exists in the literature for the last two CKM parameters, corresponding to

$$\rho + i\eta = \frac{V_{ub}^*}{V_{us}V_{cb}^*} = \left(1+\frac{1}{2}\lambda^2\right)(\bar\rho + i\bar\eta) + O(\lambda^4). \tag{5}$$

The CKM matrix can be expanded in powers of the small parameter λ (which corresponds to $\sin\theta_C \simeq 0.22$) (9), exploiting the unitarity of V_{CKM} to highlight its hierarchical structure. This expansion yields the following parameterization of the CKM matrix up to $\mathcal{O}\left(\lambda^6\right)$:

$$V_{\text{CKM}} = \begin{pmatrix} 1-\frac{1}{2}\lambda^2-\frac{1}{8}\lambda^4 & \lambda & A\lambda^3(\bar\rho - i\bar\eta) \\ -\lambda+\frac{1}{2}A^2\lambda^5[1-2(\bar\rho+i\bar\eta)] & 1-\frac{1}{2}\lambda^2-\frac{1}{8}\lambda^4(1+4A^2) & A\lambda^2 \\ A\lambda^3[1-(\bar\rho+i\bar\eta)] & -A\lambda^2+\frac{1}{2}A\lambda^4[1-2(\bar\rho+i\bar\eta)] & 1-\frac{1}{2}A^2\lambda^4 \end{pmatrix}. \tag{6}$$

The CKM matrix is complex; thus, CP violation is allowed if and only if $\bar\eta$ differs from zero. To lowest order, the Jarlskog parameter measuring CP violation in a convention-independent manner (10),

$$J_{CP} \equiv \left|\Im\left(V_{i\alpha}V_{j\beta}V_{i\beta}^*V_{j\alpha}^*\right)\right| = \lambda^6A^2\bar\eta, \qquad (i\neq j, \alpha\neq\beta), \tag{7}$$

is directly related to the CP-violating parameter $\bar\eta$, as expected.

2.2. The Unitarity Triangle

To represent the knowledge of the four CKM parameters, it is useful to exploit the unitarity condition of the CKM matrix: $V_{\text{CKM}}V_{\text{CKM}}^\dagger = V_{\text{CKM}}^\dagger V_{\text{CKM}} = \mathbb{I}$. This condition corresponds to a set of 12 equations: six for diagonal terms and six for off-diagonal terms. In particular, the equations for the off-diagonal terms can be represented as triangles in the complex plane, all characterized by the same area $J_{CP}/2$. Only two of these six triangles have sides of the same order of magnitude, $\mathcal{O}(\lambda^3)$ (i.e., are not squashed):

$$\underbrace{V_{ud}V_{ub}^*}_{\mathcal{O}(\lambda^3)} + \underbrace{V_{cd}V_{cb}^*}_{\mathcal{O}(\lambda^3)} + \underbrace{V_{td}V_{tb}^*}_{\mathcal{O}(\lambda^3)} = 0, \qquad \underbrace{V_{ud}V_{td}^*}_{\mathcal{O}(\lambda^3)} + \underbrace{V_{us}V_{ts}^*}_{\mathcal{O}(\lambda^3)} + \underbrace{V_{ub}V_{tb}^*}_{\mathcal{O}(\lambda^3)} = 0. \tag{8}$$

Figure 1 depicts these two triangles in the complex plane. In particular, the triangle defined by the former equation and rescaled by a factor $V_{cd}V_{cb}^*$ is commonly referred to as the unitarity triangle

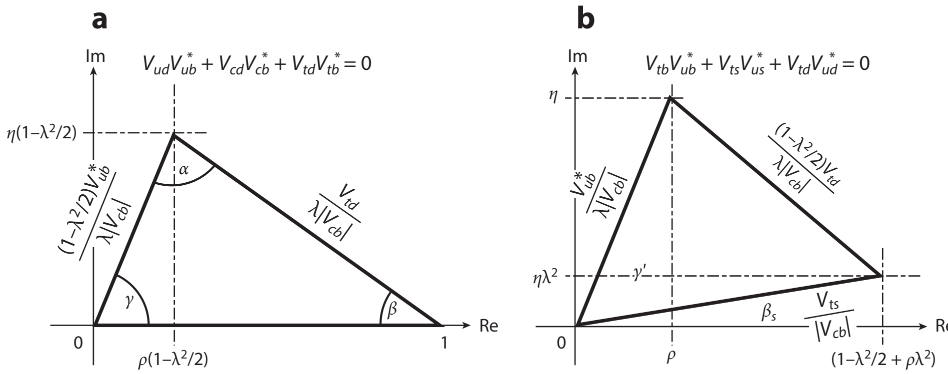

Figure 1

Representation in the complex plane of the nonsquashed triangles obtained from the off-diagonal unitarity relations of the CKM matrix (Equation 8). (*a*) The three sides are rescaled by $V_{cd}V_{cb}^*$. (*b*) The three sides are scaled by $V_{us}V_{cb}^*$.

(UT). The sides of the UT are given by

$$R_u \equiv \left|\frac{V_{ud}V_{ub}^*}{V_{cd}V_{cb}^*}\right| = \sqrt{\bar{\rho}^2 + \bar{\eta}^2}, \qquad R_t \equiv \left|\frac{V_{td}V_{tb}^*}{V_{cd}V_{cb}^*}\right| = \sqrt{(1-\bar{\rho})^2 + \bar{\eta}^2}. \tag{9}$$

The parameters $\bar{\rho}$ and $\bar{\eta}$ are the coordinates in the complex plane of the nontrivial apex of the UT, the others being (0, 0) and (1, 0). *CP* violation in the quark sector ($\bar{\eta} \neq 0$) is translated into a nonflat UT. The angles of the UT are related to the CKM matrix elements as

$$\alpha \equiv \phi_2 \equiv \arg\left(-\frac{V_{td}V_{tb}^*}{V_{ud}V_{ub}^*}\right) = \arg\left(-\frac{1-\bar{\rho}-i\bar{\eta}}{\bar{\rho}+i\bar{\eta}}\right), \tag{10}$$

$$\beta \equiv \phi_1 \equiv \arg\left(-\frac{V_{cd}V_{cb}^*}{V_{td}V_{tb}^*}\right) = \arg\left(\frac{1}{1-\bar{\rho}-i\bar{\eta}}\right), \tag{11}$$

$$\gamma \equiv \phi_3 \equiv \arg\left(-\frac{V_{ud}V_{ub}^*}{V_{cd}V_{cb}^*}\right) = \arg(\bar{\rho}+i\bar{\eta}). \tag{12}$$

The above equations show the two coexisting notations in the literature. Because it involves the CKM matrix $V_{Ud}V_{Ub}^*$ (where $U = u, c, t$), the UT arises naturally in discussion of B^0 meson transitions.

The second nonsquashed triangle has similar characteristics with respect to the UT, but it involves $V_{uD}V_{tD}^*$ (where $D = d, s, b$) and is not immediately associated with a neutral meson. One can define a modified triangle (**Figure 1**) in which all sides are rescaled by $V_{us}V_{cb}^*$. Up to $O(\lambda^4)$ corrections, its apex is located at the point (ρ, η), and it is tilted with respect to the horizontal axis by an angle

$$\beta_s \equiv \arg\left(-\frac{V_{ts}V_{tb}^*}{V_{cs}V_{cb}^*}\right) = \lambda^2\bar{\eta} + \mathcal{O}(\lambda^4). \tag{13}$$

As mentioned above, neutral mesons with other flavor content (B_s^0, D^0, K^0) would correspond to other squashed triangles with the same area and with some of their angles related to those defined above. For instance, β_s occurs naturally in the B_s^0 unitarity triangle defined from $V_{Us}V_{Ub}^*$ (where $U = u, c, t$). All these representations are particular two-dimensional projections of the four parameters describing the CKM matrix, which can be constrained through the combination of experimental and theoretical information.

3. INDIVIDUAL CONSTRAINTS

3.1. Types of Constraints

Due to its economical structure in terms of only four parameters and its consequences for *CP* violation, the CKM matrix can be determined through many different quark transitions. These correspond to $\Delta F = 1$ decays or $\Delta F = 2$ processes related to neutral-meson mixing.

Extensive measurements have been performed on K, D, and B mesons at different experiments. Constraints coming from K mesons or unflavored particles have been obtained mostly from dedicated experiments, among which NA48 (11), KLOE (12, 13), and KTeV feature prominently. Measurements of CKM parameters from D and B mesons were pioneered by ARGUS (14) at DESY, CLEO, and CLEO-c (15) at Cornell, followed by the so-called B factory experiments BaBar (16) at SLAC and Belle (17) at KEK. They operated primarily at a center-of-mass energy corresponding to the mass of the $\Upsilon(4S)$ resonance. Significant contributions also came from the CDF and D0 experiments at FNAL (18), especially those involving B_s^0 mesons, which are not accessible at the $\Upsilon(4S)$ resonance. These experiments have been terminated, whereas Belle is being upgraded (19). Physics with b and c hadrons is now dominated by the LHCb experiment (20) at the LHC. The general-purpose detector experiments ATLAS (21) and CMS (22) contribute in selected areas, and the BESIII experiment (23) also provides many results for charm hadrons.

A given experimental measurement is related to an amplitude that sums several terms, each containing CKM factors multiplied by quantities describing the quark transition and the hadronization of quarks into observable mesons or baryons. Whether a given process is relevant to measurements of the CKM parameters depends on the experimental and theoretical accuracy that can be reached. Due to the complexity of long-distance strong interactions, it is easier to select processes with a limited number of hadrons in the initial or final state, or to select observables (typically ratios) for which uncertainties due to long-distance QCD effects cancel.

In the first case, (exclusive) *CP*-conserving processes with at most one hadron in the initial and the final state are considered. After heavy degrees of freedom (in particular, weak gauge bosons) are integrated out using the effective Hamiltonian formalism (24), the long-distance hadronic contribution can be parameterized in terms of relatively simple quantities that are accessible through theoretical tools (lattice QCD simulations, effective field theories): decay constants for leptonic decays, form factors for semileptonic decays, bag parameters (matrix elements of four-quark effective operators between a meson and its antimeson) for neutral-meson mixing. It is often useful to consider ratios of observables related by $SU(3)$ flavor symmetry, as many experimental and theoretical uncertainties decrease in such ratios. For a few (inclusive) processes, a sum over all possible final states is performed; quark–hadron duality can then be invoked to compute the effects of the strong interaction perturbatively. For this first type of observable, for which significant hadronic uncertainties must be assessed carefully, the resulting constraints are generally set on the modulus of a given CKM matrix element, and are dominated by theoretical uncertainties.

In the second case, *CP*-violating observables are devised by comparing a process and its *CP* conjugate. Because the strong interaction conserves *CP*, the same hadronic amplitudes are involved and may cancel in well-designed observables such as *CP* asymmetries, measuring *CP* violation in hadron decays involving neutral-meson mixing, or in the interference between these two types of processes. This second type of observable, from which most of the hadronic uncertainties are absent, often yields information about one particular angle of the UT, dominated by experimental uncertainties. Large *CP* asymmetries are associated with the nonsquashed UT and thus occur mainly for B meson processes (often with small branching ratios due to CKM-suppressing factors).

Table 1 A partial list of measurements generally used to determine the CKM parameters, the combination of CKM parameters constrained, and the theoretical inputs needed[a]

	Dominated by experimental uncertainties		Dominated by theoretical uncertainties	
	Process	Constraint	Process	Constraint
Tree	$B \to D^{(*)}K^{(*)}$	γ	$B \to D^{(*)}\ell\nu$ $B \to X_c\ell\nu$ $B \to \pi\ell\nu$ $B \to X_u\ell\nu$ $M \to \ell\nu$ $M \to N\ell\nu$	$\lvert V_{cb}\rvert$ versus form factor $F^{B\to D^{(*)}}$ $\lvert V_{cb}\rvert$ versus OPE $\lvert V_{ub}\rvert$ versus form factor $F^{B\to\pi}$ $\lvert V_{ub}\rvert$ versus OPE $\lvert V_{UD}\rvert$ versus decay constant f_M $\lvert V_{UD}\rvert$ versus form factor $F^{M\to N}$ or $M \to N$ amplitude
Loop	$B \to (c\bar{c})K^{(*)}$ $B \to \pi\pi, \rho\pi, \rho\rho$ $B_s^0 \to J/\psi\phi$	β α β_s	ϵ_K ($K\overline{K}$ mix) Δm_d (B^0 $\overline{B}^0$ mix) Δm_s (B_s^0 $\overline{B}_s^0$ mix)	$V_{ts}V_{td}^*$ and $V_{cs}V_{cd}^*$ versus bag parameter B_K $\lvert V_{tb}V_{td}^*\rvert$ versus bag parameter B_{B^0} $\lvert V_{tb}V_{ts}^*\rvert$ versus bag parameter $B_{B_s^0}$

[a]The measurements are classified according to the dominant type of uncertainties (experimental or theoretical) and the type of processes involved (tree or loop). Abbreviation: OPE, operator product expansion.

Table 1 summarizes the processes for which a good accuracy can be reached both experimentally and theoretically. These processes are used to assess the validity of the Kobayashi–Maskawa mechanism for *CP* violation and to perform the metrology of the CKM parameters, assuming the validity of the SM. Note that $\Delta F = 2$ meson mixing corresponds to a flavor-changing neutral current, and as such, it is forbidden at tree level and is only mediated by loop processes in the SM. By contrast, $\Delta F = 1$ decays can be either related to tree processes (typically, leptonic and semileptonic decays) or involve loop processes (such as hadronic decays).

The potential sensitivity to physics beyond the SM is not the same for all processes: When discussing potential NP effects, it is often interesting to perform the metrology of the CKM matrix using only tree-level processes (this is possible by use of the unitarity of the CKM matrix and the fact that CKM moduli, apart from V_{td} and V_{ts}, can all be measured from tree-level decays) and to exploit loop processes in order to constrain additional NP effects. One may also consider additional ultrarare decays and processes that are not experimentally measured with sufficient accuracy to constrain the CKM matrix in the SM, but are very sensitive to NP—for instance, the rare $B_s^0 \to \mu\mu$ and $K \to \pi\nu\nu$ decays or the B_s^0 width difference $\Delta\Gamma_s$. This issue is discussed further in Section 4.2.

3.2. Moduli from Leptonic and Semileptonic Decays $\Delta F = 1$

The moduli described in the following subsections can be determined accurately from (*CP*-averaged) branching ratios of exclusive leptonic and semileptonic decays.

3.2.1. Transitions among the first and second generations.

The CKM matrix element $|V_{us}|$ is efficiently constrained by $K^- \to \ell^-\overline{\nu}$, $K \to \pi\ell\overline{\nu}$ and $\tau \to K^0\nu_\tau$ decays (25). Decay constants and form factors are known from lattice QCD simulations (26), whereas radiative corrections have been determined with a high accuracy on the basis of chiral perturbation theory (27).

The matrix elements $|V_{cd}|$ and $|V_{cs}|$ are constrained by D, D^+, and D_s^+ leptonic and semileptonic decays. The precision of the leptonic decays (28–31) [where the lepton is often a muon but can be a τ lepton in the case of the D_s^+ meson (31–33)] is dominated by experimental uncertainties. Conversely, the semileptonic $D \to K\ell\nu$ and $D \to \pi\ell\nu$ decays (34–38) have not been investigated by many lattice QCD collaborations, and their systematic uncertainties are expected to be improved to yield relevant constraints for the CKM parameters (26). Moreover, radiative corrections still need to be investigated in detail for these processes (39, 40).

In principle, $|V_{ud}|$ could be determined by many processes, such as $\pi^+ \to e^+\nu$, $\pi^+ \to \pi^0 e^+\nu$, and $n \to pe^-\bar{\nu}$. Yet they exhibit poor experimental accuracy for our purposes (pion leptonic or semileptonic decays), or their measurements in different experimental settings are not compatible and cannot be averaged meaningfully (neutron lifetime) (25). It turns out that the most accurate determination comes from nuclear superallowed $0^+ \to 0^+$ β decays (41). The current determination is based on a large set of nuclei and relies on sophisticated estimates of different corrections (electroweak radiative, nuclear structure, isospin violation) from dedicated nuclear physics approaches.

3.2.2. $|V_{ub}|$ and $|V_{cb}|$. The determination of the CKM matrix elements $|V_{ub}|$ and $|V_{cb}|$ provides important closure tests of the UT. It is best performed in semileptonic $b \to (u,c)\ell\nu$ decays ($\ell = e, \mu$), where there are no hadronic uncertainties related to the decay of the emitted W boson. Unfortunately, a well-known discrepancy exists between the determinations obtained from exclusive decays and from inclusive modes (42), which are treated with different tools. In the case of V_{cb}, there is no complete lattice QCD determination of the $B \to D^{(*)}\ell\nu$ form factors, which are required in order to analyze the corresponding experimental exclusive measurements (42–45). Heavy-quark effective theory (HQET) is required, expanding the form factors in powers of $1/m_b$ and $1/m_c$ in order to simplify their expression and constrain their dependence on the lepton energy, complemented with lattice QCD estimates of some of the HQET parameters. For the inclusive decay $B \to X_c\ell\nu$ (46–49), operator product expansion (OPE) (50, 51) allows the decay rate to be expressed as a series in $1/m_b$ and $1/m_c$ (52), with matrix elements that can be fitted from leptonic and hadronic moments of the branching ratio (53).

In the case of $|V_{ub}|$, the exclusive determination benefits from lattice QCD computations for the vector form factors of the decay $B \to \pi\ell\nu$ (54–56), which can be combined with measurements of the differential decay rate (42, 57–59) in order to determine V_{ub}. The inclusive determination (60–64) is more challenging. The full decay rate cannot be accessed, because a cut in the lepton energy must be performed to eliminate the huge $b \to c\ell\nu$ background. The OPE must be modified, introducing poorly known shape functions describing the b quark dynamics in the B meson (65–71). They can be constrained partly from $B \to X_s\gamma$ and raise questions concerning the convergence rate of the series in $1/m_b$ (72).

These determinations lead to a long-standing discrepancy between inclusive and exclusive determinations for $|V_{ub}|$ and $|V_{cb}|$. Currently, global fits (discussed in Section 4) use averages of both kinds of determination as inputs, but their outcome favors exclusive measurements for $|V_{ub}|$ and inclusive measurements for $|V_{cb}|$ (**Figure 2**).

Additional decay modes need to be added in order to obtain a global picture for $|V_{ub}|$ and $|V_{cb}|$. The leptonic decay $B \to \tau\nu_\tau$ has been studied at B factories (73–76), favoring values closer to the inclusive determination. The value of this branching ratio used to be at odds with expectations from global fits (77), but recent determinations from Belle reduced the discrepancy to 1.2σ. In addition, the LHCb Collaboration recently used Λ_b^0 baryon decays for the first time (78). The decay rates of $\Lambda_b^0 \to p\mu^-\nu$ and $\Lambda_b^0 \to \Lambda_c^+\mu^-\nu$ are compared to determine the ratio $|V_{ub}/V_{cb}|$, using the available lattice QCD estimates of the six different form factors involved (79). **Figure 2** depicts the overall situation, including the constraints from inclusive and exclusive determinations of $|V_{ub}|$, $|V_{cb}|$, and $|V_{ub}/V_{cb}|$.

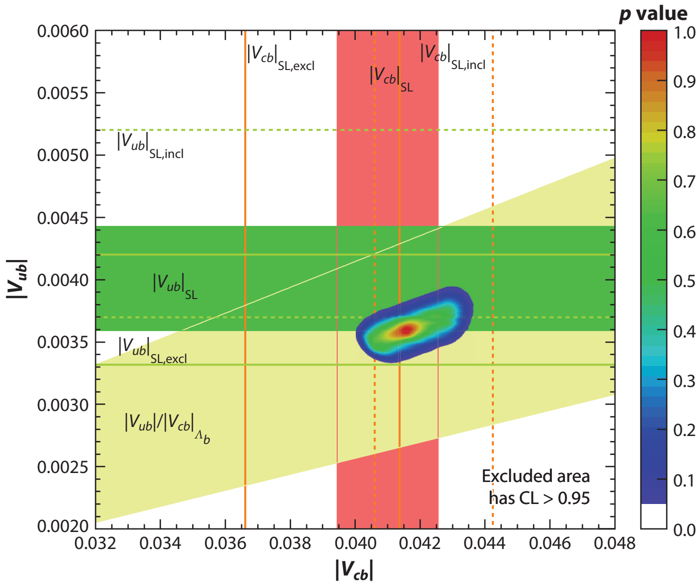

Figure 2

Experimental situation for $|V_{ub}|$ and $|V_{cb}|$. The experimental measurements from exclusive (inclusive) measurements are represented by bands with solid (dashed) lines, and their average is represented by the colored bands. The yellow diagonal band corresponds to the constraint from Λ_b^0 decays. The oval region indicates the 95%-CL region is the indirect determination of $|V_{ub}|$ and $|V_{cb}|$ from a global fit including none of these measurements. Modified from CKMfitter Group (manuscript in preparation; summer 2016 update at **http://ckmfitter.in2p3.fr**).

3.2.3. $|V_{tb}|$, $|V_{td}|$, and $|V_{ts}|$. The measurement of $|V_{tb}|$ can be performed from the cross section for single top quark production. The combination of Tevatron and LHC data yields $|V_{tb}| = 1.021 \pm 0.032$ (80), which is not competitive within the SM with the very accurate determination based on unitarity and other constraints on the CKM parameters. Other, less stringent constraints on $|V_{tb}|$ can be obtained from the ratio of branching ratios $\mathrm{Br}(t \to Wb)/\mathrm{Br}(t \to Wq)$ and from LEP electroweak precision measurements. In principle, the matrix elements $|V_{td}|$ and $|V_{ts}|$ can be measured directly from tree-level decays of top quarks (81), but the results are not competitive with neutral-meson mixing within the SM (see Section 3.4).

3.3. Unitary Triangle Angles from *CP*-Violating Measurements

The UT angles described in the following subsections can be determined experimentally from *CP*-violating measurements with almost no theoretical uncertainties.

3.3.1. The angle $\beta \equiv \varphi_1$. The mode that allowed for the first observation of *CP* violation in B decays is $B^0 \to J/\psi\, K_S^0$ (82, 83). It provides access to φ_d (84), the relative phase between the decay of the B^0 meson to $J/\psi\ K_S^0$ and that of the oscillation of B^0 to its antiparticle $\bar{B}^0$, followed by the decay $\bar{B}^0 \to J/\psi\, K_S^0$. The measurement requires studying how the decay depends on the time between the initial production of B^0 and its decay, leaving time for evolution and potential mixing between B^0 and $\bar{B}^0$ mesons. In the SM, the decay is dominated by a single CKM phase, up to Cabibbo-suppressed penguin contributions, whereas B^0 mixing is completely dominated by top–top box diagrams. Considering these two amplitudes, the measurement of the time dependence of this process yields $\sin 2\beta$ (85, 86). The B factories were optimized for this measurement (87–89) and determined (42) $\sin 2\beta^{\text{B-fact}} = 0.682 \pm 0.019$, which is the most precise constraint on the UT (**Figure 6**, below). Recently, LHCb joined the effort, publishing its first measurement of the time-dependent CP asymmetry in the decay $B^0 \to J/\psi\, K^0_S$ (90) with an uncertainty competitive with the individual measurements from the B factories. The degeneracies among the values of β are lifted thanks to the $B^0 \to J/\psi K^{*0}$ mode (91, 92), where the interferences between the difference partial waves are sensitive to $\cos 2\beta$.

The measured value for $\sin 2\beta$ is slightly lower than the expectation from all other constraints on the UT (93; CKMfitter Group, manuscript in preparation), $\sin 2\beta^{\text{indirect}} = 0.740^{+0.020}_{-0.025}$, which could be due to the so-far-neglected contribution from penguin topologies in the decay $B^0 \to J/\psi\, K^0_S$ or in other $b \to c\bar{c}s$ decays to CP eigenstates. There have been several theoretical attempts to estimate this contribution. One possibility consists of using $SU(3)$ symmetry and assessing the size of penguin contributions from $B^0 \to J/\psi\, \pi^0$, $B^0 \to J/\psi\, \rho^0$, and $B^0_s \to J/\psi\, K^0_S$ decays (94, 95); unfortunately, the accuracy of any constraints from these studies is currently limited due to the experimental inputs (96–99). By contrast, a fit to $B \to J/\psi\, P$ (where P is a light pseudoscalar meson) including $SU(3)$ breaking corrections suggests a small contamination from penguin contributions (100). Direct computations based on soft-collinear effective theory arguments (101) reach a similar conclusion. The final average of all charmonium data yields the very accurate value $\sin 2\beta^{\text{meas}} = 0.691 \pm 0.017$ (42).

The value of $\sin 2\beta$ can also be determined in $b \to q\bar{q}s$ transitions (where $q = d, s$) as $B^0 \to \eta' K^0$ (102, 103). These transitions are not allowed at tree level and thus probe the CKM mechanism in loop-induced processes, although contamination from penguins with other CKM phases is difficult to assess in these modes (104). The naïve average of all measurements results in $\sin 2\beta^{q\bar{q}s} = 0.655 \pm 0.032$ (42), which is consistent with expectations.

Crucial to this and other time-dependent measurements is the ability to identify the flavor of the B meson, before it starts its evolution and mixes with its antiparticle. Whereas so-called flavor tagging had a high efficiency at B factories (87), at the LHC the complicated hadronic environment makes this task very challenging. The tagging performance at LHCb has continuously improved over the years thanks to both a better understanding of the underlying event and the use of modern machine learning techniques (105–108). These improvements, in combination with data from the upcoming LHC Run 2, will enable further reduced uncertainties.

3.3.2. The angle $\alpha \equiv \varphi_2$. A precise determination of the UT angle α is challenging at both the theoretical and experimental levels. It requires the time-dependent study of $b \to u$ transitions as in $B \to \pi\pi$, $B \to \rho\pi$, or $B \to \rho\rho$, which are affected by $b \to d$ or $b \to s$ penguin topologies, depending on the final state considered. The interference between B^0–$\overline{B}^0$ mixing and decay amplitudes would provide a measurement of $\pi - \beta - \gamma = \alpha$ (using unitarity) in the absence of penguin contributions. In practice, this penguin pollution is present and must be constrained by determining the magnitude and the relative phases of hadronic amplitudes before determining the angle α, with the help of isospin symmetry (109, 110). For $B \to \pi\pi$ (111–117), all three possible channels are considered, and isospin symmetry can be used to relate the hadronic amplitudes, leading to triangular relations. From the measurements of branching ratios and CP asymmetries, two triangles can be reconstructed for B^+, B^0 and B^-, $\overline{B}^0$ decays, respectively, with a relative angle corresponding to α, up to discrete ambiguities. For the decay $B \to \rho\rho$ (118–124), a similar construction can be invoked for the (dominant) longitudinal polarization; interestingly, the penguin

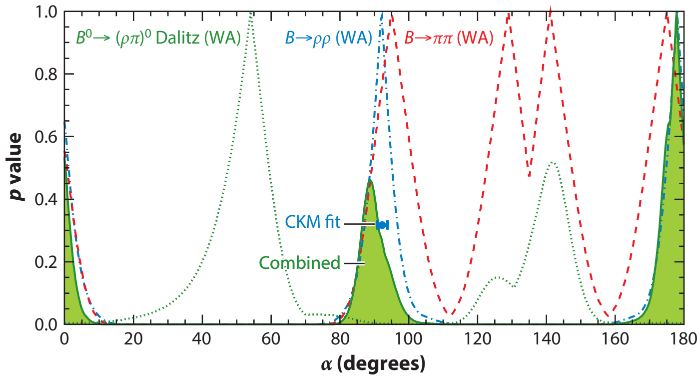

Figure 3

Constraints on the CKM angle α from $B \to \pi\pi$, $B \to \rho\pi$, and $B \to \rho\rho$. The combination of the constraints and the outcome of the global fit are also represented. Modified from CKMfitter Group (130a; manuscript in preparation; summer 2016 update at **http://ckmfitter.in2p3.fr**).

contamination turns out to be less important than for $\pi\pi$ modes. The decay $B \to \rho\pi$ (123–127) requires a more elaborate analysis: Isospin symmetry yields pentagonal relations, whereas the time-dependent $B \to \pi\pi\pi$ Dalitz plot analysis provides a large set of observables, corresponding to the parameterization of the amplitude together with an isobar model involving the ρ line shape. So far, a Dalitz plot analysis has been reported only for the $B^+ \to \pi^+\pi^-\pi^+$ decay mode (128). The present average of these constraints yields $\alpha^{\mathrm{meas}} = (88.8^{+2.3}_{-2.3})^\circ$ (CKMfitter Group, manuscript in preparation).

Figure 3 depicts the different constraints and shows the discrete symmetries present in the $\pi\pi$ and $\rho\rho$ cases, as well as the fact that two solutions are allowed by the combination of the measurements. In addition to the statistical uncertainties of the measurements, the accuracy is limited by two main hypotheses: $\Delta I = 3/2$ contributions coming from electroweak penguins are neglected, and isospin symmetry in strong interactions is not perfect (129–130a).

3.3.3. The angle $\gamma \equiv \varphi_3$. The angle γ can be obtained from tree-dominated $B \to DK$ decays, where the CP-violating phase appears in the interference of $b \to c$ (color-allowed) and $b \to u$ (color-suppressed) topologies, followed by carefully chosen D decay processes. This is the least precisely known angle of the UT, and its determination from tree decays is considered to be free from contributions beyond the SM and unaffected by hadronic uncertainties, contrary to the angles α and β (131). There is still great potential for the improvement of the measurement of γ by several order of magnitudes compared with the theoretical uncertainties. The angle γ can thus provide a reference to which other measurements of the CKM parameters can be compared both within the SM and beyond.

Three different methods have been devised in order to obtain information on γ, depending on the subsequent decays of $D^{(*)}$ mesons, with a different sensitivity to the ratio of color-favored and color-suppressed amplitudes. The Gronau–London–Wyler (GLW) method (132, 133) considers the decay of the D meson into CP eigenstates, eliminating further hadronic uncertainties concerning the D decays. The Atwood–Dunietz–Soni (ADS) method (134, 135) considers decays of the $D^{(*)}$ meson with a pattern of Cabibbo dominance/suppression that counteracts the color suppression/dominance of the B decay, for instance, $D \to K^{\mp}\pi^{\pm}$. Finally, the

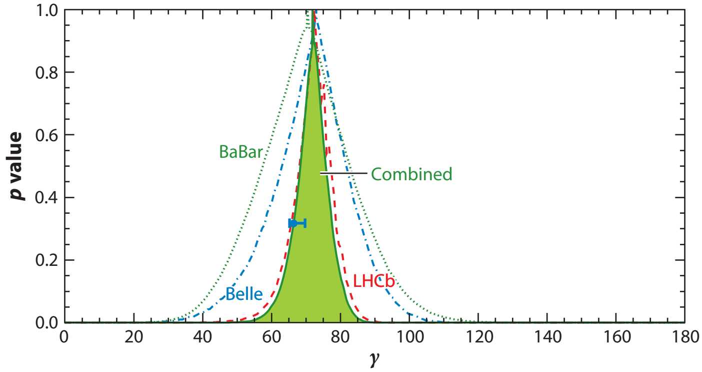

Figure 4

Constraints on the CKM angle γ from the BaBar, Belle, and LHCb experiments. Modified from CKMfitter Group (manuscript in preparation; summer 2016 update at **http://ckmfitter.in2p3.fr**).

Giri–Grossman–Soffer–Zupan (GGSZ) method (136) performs a Dalitz analysis of three-body $D^{(*)}$ decays, inducing a dependence on the amplitude model for $D^{(*)}$ decays.

The last two methods require additional information about the strong phase structure in multi-body D decays, which was provided by CLEO-c (137–139). LHCb has performed several measurements using the GLW/ADS (140–144) and GGSZ (145, 146) methods with various B^0 and B^+ decays, as well as a time-dependent $B_s^0 \to D_s^{\pm} K^{\mp}$ analysis (147, 148). As some systematic uncertainties are correlated among analyses, LHCb has performed a combination yielding $\gamma = (72.2^{+6.8}_{-7.3})°$ (149).

Similarly, the B factories BaBar and Belle have performed combinations of their measurements (150, 151) and obtained $\gamma = (67 \pm 11)°$ (87). The combination of the values for γ yields $\gamma^{\mathrm{meas}} = (72.1^{+5.4}_{-5.8})°$, with the confidence-level curves shown in **Figure 4**. Because there is no irreducible theoretical uncertainty on the determination of γ (131), there is plenty of room for more precision measurements of this quantity.

3.3.4. The angle φ_s. By analogy with the measurement of $\sin 2\beta$ related to B^0 mixing, a CP-violating phase φ_s related to B_s^0 mixing can be determined through time-dependent measurements of $b \to c\bar{c}s$ decays. This phase is equal to $-2\beta_s \equiv -2\arg[-V_{ts}V_{tb}^*/V_{cs}V_{cb}^*] = -0.0370^{0.0006}_{0.0007}$ rad in the SM (CKMfitter Group, manuscript in preparation), neglecting subleading penguin contributions. This phase has been measured using the decay $B_s^0 \to J/\psi\,\phi$ with $J/\psi \to \mu^+\mu^-$ and $\phi \to K^+K^-$ by CDF (152), D0 (153), CMS (154), and ATLAS (155). LHCb uses the decay $B_s^0 \to J/\psi\,K^+K^-$ (including $B_s^0 \to J/\psi\,\phi$) in a polarization-dependent way (156), as well as the pure CP-odd decay $B_s^0 \to J/\psi\,\pi^+\pi^-$ (157, 158). **Figure 5** shows the current constraints on φ_s and the decay width difference $\Delta\Gamma_s = \Gamma_L - \Gamma_H$.

Similarly to the case for the angle β, the SM prediction $\varphi_s^{c\bar{c}s} = -2\beta_s$ assumes tree-dominated decays. With the increasing precision on the CKM parameters, the effects of suppressed penguin topologies can no longer be neglected (95, 162–166). Cabibbo-suppressed decay modes, in which these topologies are relatively more prominent, can be used to constrain such effects. Methods of using selected measurements constraining the sizes of penguin amplitudes have been described elsewhere (94, 100, 101, 167, 168). The LHCb Collaboration is pursuing this program with studies of the decays $B_s^0 \to J/\psi\,K_S^0$ (169) and $B_s^0 \to J/\psi\,\overline{K}^{*0}$ (170).

Another interesting test of the SM is provided by the measurement of the mixing phase $\varphi_s^{s\bar{s}s}$ with the penguin-dominated mode $B_s^0 \to \phi\phi$. In this case, the measured value is $-0.17 \pm 0.15 \pm 0.03$ rad (171), which is compatible with the SM expectation.

3.4. Information from $\Delta F = 2$ Transitions

$\Delta F = 2$ transitions are particularly useful both in the SM and in the search for NP, as these are flavor-changing neutral currents arising only as loops in the SM. Among the four neutral mesons available, the K^0, B^0, and B_s^0 systems are useful for the metrology of the SM. Indeed, the mixing of the charm meson D^0 is notoriously difficult to estimate theoretically because, due to the Glashow–Iliopoulos–Maiani (GIM) mechanism, it is dominated by the first two generations, and thus by long-distance QCD dynamics (172).

3.4.1. B^0 and B_s^0 systems. Due to neutral-meson oscillation, the flavor eigenstates P^0 and $\bar{P}^0$ mix into the mass eigenstates P_L and P_H, denoting, respectively, the light and heavy mesons. This language is used to describe several observables for the B^0 and B_s^0 systems: the mass difference $\Delta m = M_H - M_L$, the width difference $\Delta\Gamma = \Gamma_L - \Gamma_H$, and the semileptonic asymmetry $a_{\mathrm{SL}}^{d,s}$ that measures *CP* violation in mixing by comparing semileptonic decays of P^0 or $\bar{P}^0$ into "wrong-sign" leptons (such processes can occur only if P_0 or $\bar{P}_0$ mixes into its antiparticle). Due to the pattern of CKM factors (suppressing charm contributions), Δm is dominated by the dispersive part of top quark–dominated box diagrams. It can be studied within an effective Hamiltonian analysis by integrating out heavy (W, Z, t, H) degrees of freedom: It amounts to a local contribution that requires the input of a single bag parameter once short-distance QCD corrections (gluon exchanges) have been taken into account (24, 173). This explains why the mass difference Δm has long been used to constrain the CKM parameters. By contrast, $\Delta\Gamma$, related to the imaginary part of the amplitude, involves only real intermediate states. Therefore, it is dominated by the absorptive part of the box diagram involving the charm quark, namely the decays of P^0 and $\bar{P}^0$ into common

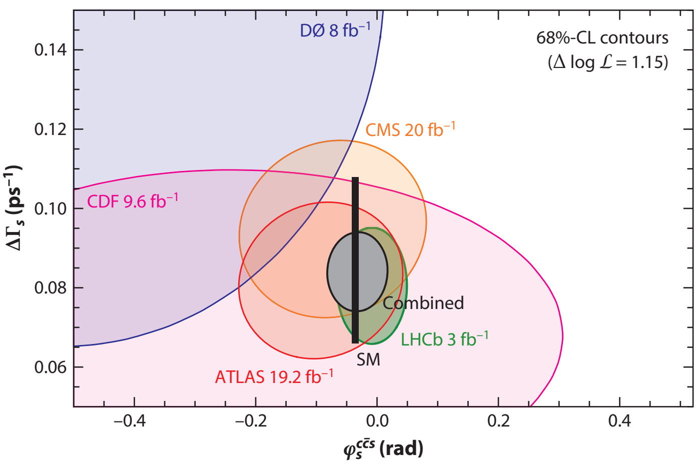

Figure 5

Constraints on $\Delta\Gamma_s$ and $\varphi_s^{c\bar{c}s}$ from various decays and experiments. The Standard Model (SM) predictions are from References 159–161. Modified from Reference 42.

final states. The evaluation of this nonlocal contribution requires a further $1/m_b$ expansion, with larger uncertainties and two hadronic bag parameters, making $\Delta\Gamma$ (and $a_{\mathrm{SL}}^{d,s}$) harder to control theoretically (77, 160, 174–177).

The frequency of B^0 and B_s^0 mixing probes $|V_{tb}V_{tq}^*|$, where $q = d$ and s, respectively. They are measured as $\Delta m_d^{\mathrm{meas}} = 506.4 \pm 1.9\,\mathrm{ns}^{-1}$ and $\Delta m_s^{\mathrm{meas}} = 17.757 \pm 0.021\,\mathrm{ps}^{-1}$ (42), placing strong constraints on the UT. The accuracy of these constraints is limited mainly by the determination of the corresponding bag parameters. It is more useful to consider the ratio $\Delta m_d/\Delta m_s$, which involves an $SU(3)$ breaking ratio of bag parameters that is known more accurately than individual quantities from lattice simulations (26).

The B_s^0 meson system has many features in common with the K^0 meson system, with a heavy long-lived and a light short-lived eigenstate. The a priori unknown admixture of the two states contributing to a given non-flavor-specific decay causes uncertainties in the measurement of branching fractions, for instance, for the decay $B_s^0 \to \mu^+\mu^-$ (178–181). Thus, a precise determination of the decay width difference is also important for the study of rare decays and efficiently constrains models of NP in $\Delta F = 2$ transitions (77, 160, 175, 182, 183).

Whereas measurements of Δm_d and Δm_s are consistent with expectations, the D0 experiment reported an unexpectedly large dimuon asymmetry (184) that differs from the SM expectation by 3σ. This measurement is generally interpreted as a combination of the semileptonic asymmetries a_{SL}^d and a_{SL}^s in B^0 and B_s^0 decays, respectively, which measure *CP* violation in mixing. Direct measurements of a_{SL}^d and a_{SL}^s at *B* factories (185–187), D0 (188, 189), and LHCb (190, 191) are consistent with the SM prediction and in tension with the D0 asymmetry. The origin of this discrepancy is still under investigation (192), as we discuss further in Section 4.2.1.

3.4.2. The K^0 system. The pattern of CKM factors requires loops involving top and charm quarks to be considered in the case of the kaon system. The mass difference Δm_K thus gets not only top box contributions but also charm–top and charm–charm contributions, which are long-distance contributions that are difficult to estimate (24, 173). A way out involves considering observables related to *CP* violation in K^0 mixing and decays into pions. In the absence of *CP* violation, only the short-lived kaon, K_{S}^0, decays into $\pi\pi$, whereas the long-lived kaon, K_{L}^0, decays into 3π. A measurement of *CP* violation can be defined from the amplitude of K_{S}^0 and K_{L}^0 states decaying into a $\pi\pi$ state with total isospin $I = 0$:

$$\epsilon_K = \frac{\langle(\pi\pi)_{I=0}|K_{\mathrm{L}}^0\rangle}{\langle(\pi\pi)_{I=0}|K_{\mathrm{S}}^0\rangle}. \qquad 14.$$

This term is related to the difference between *CP* eigenstates and mass eigenstates, and it requires a global fit to many observables describing $K \to 2\pi$ decays (25). Its real part indicates *CP* violation in mixing, and its imaginary part measures *CP* violation in the interference between mixing and decay. ϵ_K can be computed accurately in terms of short-distance (Inami–Lim) functions as well as a long-distance bag parameter, which is known from lattice QCD simulations (26). An accurate SM prediction of ϵ_K also requires a resummation of short-distance QCD corrections (gluon exchanges), encoded into η_{tt}, η_{ct}, and η_{cc}. These coefficients have been computed up to next-to-leading order (NLO) for η_{tt} (193) and next-to-next-to-leading order (NNLO) for η_{ct} and η_{cc} (194, 195), the latter of which is still affected by large theoretical uncertainties. The interpretation in terms of the CKM parameters involves A, $\bar\rho$, and $\bar\eta$ (and is thus connected with $|V_{cb}|$) and corresponds to a hyperbola in the $(\bar\rho, \bar\eta)$ plane.

Another interesting quantity is given by ϵ_K', which is defined to measure *CP* violation in decays by comparing the rates of K_{L}^0 and K_{S}^0 decay into $\pi^+\pi^-$ and $\pi^0\pi^0$. This quantity has been measured precisely (25, 196, 197) but is difficult to predict theoretically, as it receives dominant contributions from two four-quark operators (denoted Q_6 and Q_8 in the framework of the effective Hamiltonian) that largely cancel each other. A lattice QCD evaluation of all the bag parameters needed has recently been performed (198), suggesting a discrepancy between 2σ and 3σ with respect to SM expectations (198–201). This interesting but challenging issue definitely calls for estimations of the relevant bag parameters from other lattice QCD collaborations.

3.5. Lepton Flavor Universality

The metrology of the CKM parameters discussed above relies on modes that can be predicted accurately in the SM and provide information about its parameters. However, it mixes modes with different sensitivities to physics beyond the SM: on one hand, flavor-changing charged currents, such as semileptonic decays, which are dominated by tree-level processes in the SM, and on the other hand, flavor-changing neutral currents, such as neutral-meson mixing, which are mediated by loop processes in the SM. Additional, rare processes that are not expected to provide further constraints on the parameters of the SM can probe some of the underlying hypotheses at the core of this theory. More details can be found in a previous volume of this journal (202).

A particularly topical example is lepton flavor universality. In both flavor-changing charged and neural currents, the weak interaction at play deals with lepton flavors in a universal manner, whereas quarks are treated on a different footing due to the CKM matrix. This universality of lepton couplings is assumed when determining the CKM parameters, in particular to combine results from semileptonic and leptonic decays that involve e, μ, and/or τ leptons.

Recently, LHCb and the B factories found interesting hints of violation of lepton flavor universality in both flavor-changing charged and neural currents (203). The measurements in charged currents between $B\to D^{(*)}\tau\nu$ and $B\to D^{(*)}\ell\nu$, where $\ell=\mu, e$ (204–209), indicate that the ratios $R(D)$ and $R(D^*)$ exceed SM predictions by 1.9σ and 3.3σ, respectively, leading to a combined discrepancy with the SM at 4.0σ (42):

$$R_{D^{(*)}}=\frac{\mathrm{Br}(B\to D^{(*)}\tau\nu)}{\mathrm{Br}(B\to D^{(*)}\ell\bar{\nu}_\ell)}\,. \qquad 15.$$

The individual branching ratios are consistent with a 15% enhancement for $b\to c\tau\bar{\nu}_\tau$ compared with SM expectations. Several similar measurements, notably from LHCb, are ongoing and should provide a clearer picture in the near future.

The violation of lepton flavor universality has also been investigated for the flavor-changing neutral-current (FCNC) transition $b\to s\ell^+\ell^-$ at several experiments. LHCb (203) measured the observable $R_K=\mathrm{Br}(B\to K\mu^+\mu^-)/\mathrm{Br}(B\to Ke^+e^-)$ in the dilepton mass range from 1 to 6 GeV^2 as $0.745^{+0.090}_{-0.074}\pm0.036$, corresponding to a 2.6σ tension with its SM value, which is predicted to be equal to one (to high accuracy). This violation has also been studied in $B\to K^*\ell^+\ell^-$ transitions, with $R_{K^{*0}}$ measured in two low-q^2 bins with deviations from the SM between 2.2 and 2.5σ (210). Other recent experimental results have shown interesting deviations from the SM in the muon sector. The LHCb analysis (211) of the decay $B^0\to K^{*0}\mu^+\mu^-$ reports an $\sim3\sigma$ anomaly in two large K^* recoil bins of the angular observable P_5' (212). This report was subsequently confirmed by the Belle experiment (213) with the hint that it would arise in $b\to s\mu^+\mu^-$ but not in $b\to se^+e^-$ (214). Finally, the LHCb results for the branching ratio of several $b\to s\mu^+\mu^-$ decays exhibit deviations at low dilepton masses (215–218).

Confirmation of these deviations from lepton flavor universality would be an unambiguous sign of physics beyond the SM. It would also have consequences for the constraints described above, especially those in Section 3.2, which are determined using leptonic and semileptonic decays. Most analyses assume lepton universality, a hypothesis that would need to be revisited (see Section 4.2.2 for more detail).

4. GLOBAL ANALYSES

4.1. Determination of CKM Parameters

The following subsections describe how the above-mentioned individual constraints can be combined to constrain the CKM parameters.

4.1.1. Statistical approaches to global analyses. The individual constraints presented above must be combined in order to obtain statistically meaningful constraints on the CKM parameters. The problem can be described as a series of observables (e.g., branching ratios of leptonic and semileptonic decays, mass difference for neutral mesons) depending on theoretical parameters. Some of these are of interest ($A, \lambda, \bar{\rho}, \bar{\eta}$); the others are called nuisance parameters (e.g., decay constants, form factors, quark masses). The primary goal of statistical analysis is to determine the confidence intervals for the CKM parameters (and other fundamental parameters for models beyond the SM). The accuracy of the determination of the CKM parameters thus depends on the precision of the experimental measurements and on the theoretical computations of the nuisance parameters. Currently, global analyses are limited mainly by the latter, which are obtained mostly from QCD lattice simulations that consider a discretized version of QCD on a finite grid and compute correlators through Monte Carlo integrations over gluon gauge configurations. Due to the remarkable improvement in computing power and algorithms over recent decades, these computations are now dominated mainly by systematic uncertainties (extrapolation in lattice spacing, volume and quark masses, renormalization).

Therefore, a global analysis requires both a general statistical framework and a specific model for systematic uncertainties. Frequentist and Bayesian approaches have been proposed to deal with such analyses: The former defines probability as the outcome of repeated trials/measurements in the limit where their number becomes infinite, and the latter considers them as a subjective degree of credibility given by the observer to each possible result. The choice between the two approaches is the subject of considerable discussion in the literature (a specific discussion regarding the CKM case can be found in References 219–222). The frequentist approach has been adopted by the CKMfitter Group (161, 223), whereas the Bayesian approach is used by the UTfit Group (224).

Another issue, the models for systematic uncertainties, is also a matter of debate. For lack of a better choice, and even though they are not of a statistical nature by definition, systematic uncertainties are often described with the same model as statistical uncertainties, for instance, in the case of the UTfit group (224). Alternative treatments consist of determining sets of confidence intervals for specific values of the systematic uncertainties before combining them in unified confidence intervals [the scan method (225)] or building dedicated models for likelihoods and p values treating a range of values for the systematic uncertainties on an equal footing [the Rfit model used by the CKMfitter Collaboration (161)]. This choice has an effect not only when performing the global fit itself but also when choosing inputs by averaging measurements or computations from different groups. A more detailed discussion of the various models for theoretical uncertainties can be found in Reference 226.

4.1.2. Determination of the CKM parameters and consistency tests. For illustrative purposes, we use the results obtained by the CKMfitter Group, based on the results available at the

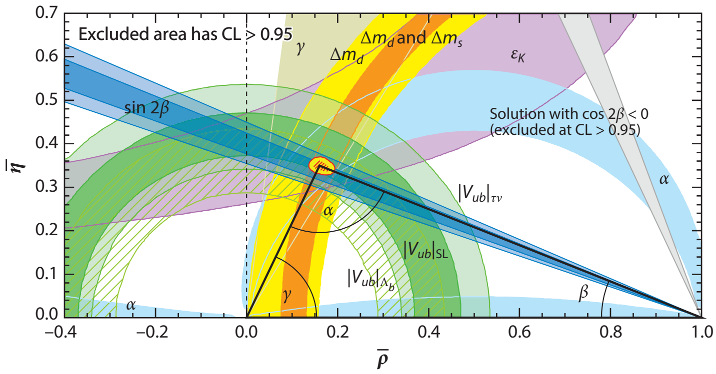

Figure 6

Status of the CKM unitarity triangle fit in $(\bar{\rho}, \bar{\eta})$ in summer 2016. Regions outside the colored areas have CL > 95.45%. For the combined fit, the yellow area inscribed by the contour line represents points with CL < 95.45%. The shaded area inside this region represents points with CL < 68.3%. Modified from CKMfitter Group (manuscript in preparation; summer 2016 update at **http://ckmfitter.in2p3.fr**).

time of the 2016 International Conference on High Energy Physics (ICHEP) (CKMfitter Group, manuscript in preparation). **Figure 6** depicts the current situation regarding the global fit in the $(\bar{\rho}, \bar{\eta})$ plane. **Table 2** lists the input parameters. As indicated in Section 2.2, this result could be cast into other UTs.

Some comments are in order before we discuss the metrology of the parameters. There exists a unique preferred region defined by the entire set of observables under consideration in the global fit. In **Figure 6**, this region is represented by the yellow surface inscribed by the red contour line for which the values of $\bar{\rho}$ and $\bar{\eta}$ with a p value such that $1 - p < 95.45\%$. The goodness of the fit must be assessed in relation to the model used to describe the theoretical uncertainties. If all of the inputs' uncertainties are assumed to be statistical in nature, and if they can be combined in quadrature, the corresponding minimal χ^2 has a p value of 20% (i.e., 1.3σ). The following values for the four parameters describing the CKM matrix are obtained:

$$A = 0.825^{+0.007}_{-0.012}, \quad \lambda = 0.2251^{+0.0003}_{-0.0003}, \quad \bar{\rho} = 0.160^{+0.008}_{-0.007}, \quad \bar{\eta} = 0.350^{+0.006}_{-0.006}. \qquad 16.$$

The overall consistency is striking when comparing constraints from tree-mediated (leptonic and semileptonic decays) and loop-mediated (e.g., neutral-meson mixing) processes, as well as processes requiring *CP* violation (such as nonvanishing *CP* asymmetries) with respect to processes taking place even if *CP* were conserved (such as leptonic and semileptonic decays) (**Figure 6**). The consistency observed among the constraints allows one to perform the metrology of the CKM parameters and to give predictions for any CKM-related observable within the SM. Each comparison between the prediction issued from the fit and the corresponding measurement constitutes a null test of the SM hypothesis.

Figure 7 shows some of the corresponding pulls, demonstrating that there is no sign of discrepancy with this set of inputs. In particular, recent discrepancies related to $B(B \to \tau\nu)$, $\sin(2\beta)$, φ_s (77), V_{cb}, ϵ_K (228, 229), or $\Delta m_{d,s}$ (230) do not appear, either because of recent changes in the experimental inputs or because of the dependence of these discrepancies on the statistical treatment and the modeling of systematic uncertainties.

Unitarity tests using direct determination of individual matrix elements (without resorting to unitarity) can also be performed by checking that the sum of their squares equals unity. For the

Table 2 Constraints used for the global fit and the main inputs involved[a]

CKM	Process	Observables			Theoretical inputs	
$\lvert V_{ud}\rvert$	$0^+ \to 0^+$ transitions	$\lvert V_{ud}\rvert_{\mathrm{nucl}}$	$= 0.97425 \pm 0 \pm 0.00022$	(41)	Nuclear matrix elements	
$\lvert V_{us}\rvert$	$K \to \pi \ell \nu$	$\lvert V_{us}\rvert_{\mathrm{SL}} f_+^{K\to\pi}(0)$	$= 0.2165 \pm 0.0004$	(25)	$f_+^{K\to\pi}(0)$	$= 0.9681 \pm 0.0014 \pm 0.0022$
	$K \to e \nu_e$	$\mathcal{B}(K \to e\nu_e)$	$= (1.581 \pm 0.008) \times 10^{-5}$	(25)	f_K	$= 155.2 \pm 0.2 \pm 0.6$ MeV
	$K \to \mu\nu_\mu$	$\mathcal{B}(K \to \mu\nu_\mu)$	$= 0.6355 \pm 0.0011$	(25)		
	$\tau \to K\nu_\tau$	$\mathcal{B}(\tau \to K\nu_\tau)$	$= (0.6955 \pm 0.0096) \times 10^{-2}$	(25)		
$\frac{\lvert V_{us}\rvert}{\lvert V_{ud}\rvert}$	$K \to \mu\nu / \pi \to \mu\nu$	$\frac{\mathcal{B}(K \to \mu\nu_\mu)}{\mathcal{B}(\pi \to \mu\nu_\mu)}$	$= 1.3365 \pm 0.0032$	(25)	f_K/f_π	$= 1.1959 \pm 0.0010 \pm 0.0029$
	$\tau \to K\nu / \tau \to \pi\nu$	$\frac{\mathcal{B}(\tau \to K\nu_\tau)}{\mathcal{B}(\tau \to \pi\nu_\tau)}$	$= (6.43 \pm 0.09) \times 10^{-2}$	(25)		
$\lvert V_{cd}\rvert$	νN	$\lvert V_{cd}\rvert_{\nu N}$	$= 0.230 \pm 0.011$	(25)		
	$D \to \mu\nu$	$\mathcal{B}(D \to \mu\nu)$	$= (3.74 \pm 0.17) \times 10^{-4}$	(42)	f_{D_s}/f_D	$= 1.175 \pm 0.001 \pm 0.004$
	$D \to \pi\ell\nu$	$\lvert V_{cd}\rvert f_+^{D\to\pi}(0)$	$= 0.1425 \pm 0.0019$	(36, 37)	$f_+^{D\to\pi}(0)$	$= 0.666 \pm 0.020 \pm 0.048$
$\lvert V_{cs}\rvert$	$W \to c\bar{s}$	$\lvert V_{cs}\rvert_{W\to c\bar{s}}$	$= 0.94^{+0.32}_{-0.26} \pm 0.13$	(25)		
	$D_s \to \tau\nu$	$\mathcal{B}(D_s \to \tau\nu)$	$= (5.55 \pm 0.24) \times 10^{-2}$	(42)	f_{D_s}	$= 248.2 \pm 0.3 \pm 1.9$ MeV
	$D_s \to \mu\nu$	$\mathcal{B}(D_s \to \mu\nu_\mu)$	$= (5.57 \pm 0.24) \times 10^{-3}$	(42)		
	$D \to K\ell\nu$	$\lvert V_{cs}\rvert f_+^{D\to K}(0)$	$= 0.7226 \pm 0.0034$	(36–38)	$f_+^{D\to K}(0)$	$= 0.747 \pm 0.011 \pm 0.034$
$\lvert V_{ub}\rvert$	Semileptonic B	$\lvert V_{ub}\rvert_{\mathrm{SL}}$	$= (3.98 \pm 0.08 \pm 0.22) \times 10^{-3}$	(42, CKMfitter Group, manuscript in preparation)	Form factors, shape functions	
	$B \to \tau\nu$	$\mathcal{B}(B \to \tau\nu)$	$= (1.08 \pm 0.21) \times 10^{-4}$	(42)	f_{B_s}/f_B	$= 1.205 \pm 0.003 \pm 0.006$
$\lvert V_{cb}\rvert$	Semileptonic B	$\lvert V_{cb}\rvert_{\mathrm{SL}}$	$= (41.00 \pm 0.33 \pm 0.74) \times 10^{-3}$	(42)	Form factors, OPE matrix elements	
$\lvert V_{ub}/V_{cb}\rvert$	Semileptonic Λ_b	$\frac{\mathcal{B}(\Lambda_p \to p\mu^-\bar{\nu}_\mu)_{q^2>15}}{\mathcal{B}(\Lambda_p \to \Lambda_c\mu^-\bar{\nu}_\mu)_{q^2>7}}$	$= (0.944 \pm 0.081) \times 10^{-2}$	(78)	$\frac{\zeta(\Lambda_p \to p\mu^-\bar{\nu}_\mu)_{q^2>15}}{\zeta(\Lambda_p \to \Lambda_c\mu^-\bar{\nu}_\mu)_{q^2>7}}$	$= 1.471 \pm 0.096 \pm 0.290$
α	$B \to \pi\pi, \rho\pi, \rho\rho$	Branching ratios, *CP* asymmetries		(42)	Isospin symmetry	
β	$B \to (c\bar{c})K$	$\sin(2\beta)_{[c\bar{c}]}$	$= 0.691 \pm 0.017$	(42)	Penguin neglected	
γ	$B \to D^{(*)}K^{(*)}$	Inputs for the three methods		(42)	GGSZ, GLW, ADS methods	
ϕ_s	$B_s \to J/\psi(KK, \pi\pi)$	ϕ_s	$= -0.030 \pm 0.033$	(42)	Penguin neglected	
$V_{tq}^* V_{tq'}$	Δm_d	Δm_d	$= 0.5065 \pm 0.0019\ \mathrm{ps}^{-1}$	(42)	$\hat{B}_{B_s}/\hat{B}_{B_d}$	$= 1.007 \pm 0.014 \pm 0.014$
	Δm_s	Δm_s	$= 17.757 \pm 0.021\ \mathrm{ps}^{-1}$	(42)	$\hat{B}_{B_s}$	$= 1.320 \pm 0.016 \pm 0.030$
	$B_s \to \mu\mu$	$\mathcal{B}(B_s \to \mu\mu)$	$= (2.8^{+0.7}_{-0.6}) \times 10^{-9}$	(180)	f_{B_s}	$= 225.1 \pm 1.5 \pm 2.0$ MeV
$V_{td}^* V_{ts}$ $V_{cd}^* V_{cs}$	ϵ_K	$\lvert\epsilon_K\rvert$	$= (2.228 \pm 0.011) \times 10^{-3}$	(25)	$\hat{B}_K$ κ_ϵ	$= 0.7567 \pm 0.0021 \pm 0.0123$ $= 0.940 \pm 0.013 \pm 0.023$

[a]When two uncertainties are quoted, the first one is statistical and the second is systematic. The lattice inputs and the averaging method used are discussed by the CKMfitter Group (manuscript in preparation), along with additional theoretical inputs (quark masses, strong coupling constant, short-distance QCD corrections for meson mixing). For a review of lattice inputs, see Reference 26. Abbreviations: ADS, Atwood–Dunietz–Soni; GGSZ, Giri–Grossman–Soffer–Zupan; GLW, Gronau–London–Wyler; OPE, operator product expansion.

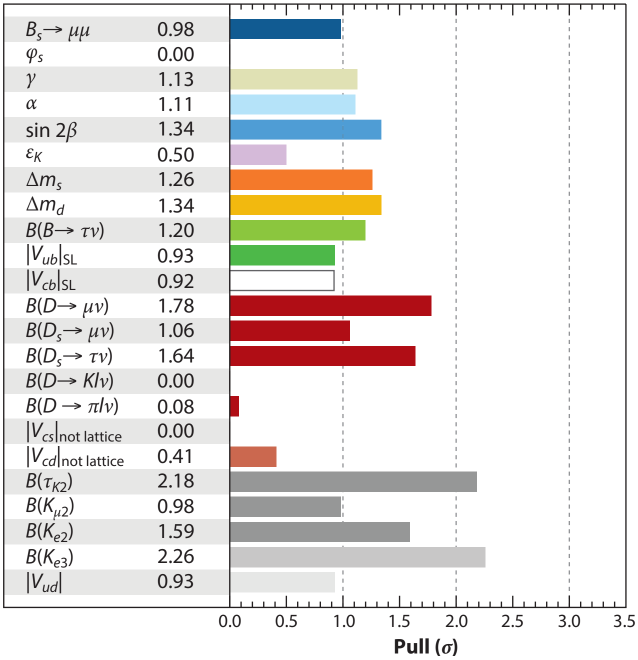

Figure 7

Pulls for the global fit in summer 2016, as defined in Reference 77 and by the CKMfitter Group (manuscript in preparation). Each pull amounts to the absolute difference between the predicted and measured values, divided by the experimental uncertainty when the latter is large compared with the uncertainty of the prediction (227). Modified from CKMfitter Group (manuscript in preparation; summer 2016 update at **http://ckmfitter.in2p3.fr**).

first two rows of the CKM matrix, the following results are obtained

$$|V_{ud}|^2_{\text{meas}} + |V_{us}|^2_{\text{meas}} + |V_{ub}|^2_{\text{meas}} - 1 = -0.0006^{+0.0006}_{-0.0002}, \tag{17}$$

$$|V_{cd}|^2_{\text{meas}} + |V_{cs}|^2_{\text{meas}} + |V_{cb}|^2_{\text{meas}} - 1 = -0.0034^{+0.0048}_{-0.0026}, \tag{18}$$

where each "measured" value includes all semileptonic and leptonic direct determinations of a given CKM matrix element (an average of inclusive and exclusive semileptonic measurements is used for the semileptonic input for $|V_{ub}|$ and $|V_{cb}|$). No deviation from unitarity is observed. There is no direct determination of $|V_{td}|$ and $|V_{ts}|$ (they are obtained from $\Delta F = 2$ loop processes), and there is no accurate direct determination of $|V_{tb}|$ (25); thus, no equivalent test can be performed for the third row or any of the columns of the CKM matrix. Similarly, the value of $\alpha + \beta + \gamma$ cannot be probed directly, because the determination of α from $B \to \pi\pi, \pi\rho, \rho\rho$ already assume unitarity.

The global fit also provides indirect predictions (i.e., not including direct measurements of these quantities) for quantities of interest, either measured experimentally or determined from lattice QCD simulations (**Table 3**). A similar level of accuracy is achieved for some observables in both their direct determinations and their indirect prediction. Improving their measurement will have only a limited impact on the fit, unless the central value differs significantly from the global fit expectations (which would then require a fine understanding of all sources of uncertainties of the

Table 3 A few predictions from the global fit (indirect, i.e., not including direct determinations of these quantities) compared with direct determinations[a]

Quantity	Fit prediction	Direct determination
α (°)	$92.1^{+1.5}_{-1.1}$	$88.8^{+2.3}_{-2.3}$
β (°)	$23.7^{+1.1}_{-1.0}$	$21.8^{+0.7}_{-0.7}$
γ (°)	$65.3^{+1.0}_{-2.5}$	$72.1^{+5.4}_{-5.8}$
φ_s (rad)	$-0.0370^{+0.0006}_{-0.0007}$	-0.030 ± 0.033
$\mathrm{Br}(B_s^0 \to \mu^+\mu^-) \times 10^9$	$3.36^{+0.07}_{-0.19}$	$2.62^{+0.66}_{-0.56}$
$\mathrm{Br}(B^0 \to \mu^+\mu^-) \times 10^{11}$	$9.55^{+0.25}_{-0.44}$	–
$V_{ub} \times 10^3$	$3.60^{+0.10}_{-0.10}$	$3.98 \pm 0.08 \pm 0.22$
$V_{cb} \times 10^3$	$42.2^{+0.7}_{-0.7}$	$41.00 \pm 0.33 \pm 0.74$
f_K	$0.15652^{+0.00013}_{-0.00020}$	$0.1552 \pm 0.0002 \pm 0.0006$
f_K/f_π	$1.1965^{+0.0021}_{-0.0063}$	$1.1959 \pm 0.0010 \pm 0.0029$
$f_+^{K\to\pi}(0)$	$0.9602^{+0.0020}_{-0.0025}$	$0.9681 \pm 0.0014 \pm 0.0022$
$\hat{B}_K$	$0.79^{+0.17}_{-0.11}$	$0.7567 \pm 0.0021 \pm 0.0123$
f_{D_s} (GeV)	$0.2512^{+0.0032}_{-0.0032}$	$0.2482 \pm 0.0003 \pm 0.0019$
f_{D_s}/f_D	$1.226^{+0.029}_{-0.027}$	$1.175 \pm 0.001 \pm 0.004$
$f_+^{D\to\pi}(0)$	$0.633^{+0.009}_{-0.008}$	$0.666 \pm 0.020 \pm 0.048$
$f_+^{D\to K}(0)$	$0.742^{+0.004}_{-0.004}$	$0.747 \pm 0.011 \pm 0.034$
$f_{B_s^0}$ (GeV)	$0.226^{+0.004}_{-0.005}$	$0.2251 \pm 0.0015 \pm 0.0020$
$f_{B_s^0}/f_B$	$1.243^{+0.027}_{-0.020}$	$1.205 \pm 0.003 \pm 0.006$
$\hat{B}_{B_s^0}$	$1.332^{+0.040}_{-0.067}$	$1.320 \pm 0.016 \pm 0.030$
$\hat{B}_{B_s^0}/\hat{B}_{B^0}$	$1.114^{+0.046}_{-0.047}$	$1.007 \pm 0.014 \pm 0.014$

[a]The top panel corresponds to experimental inputs; the bottom panel to inputs from lattice QCD computations. In the case of $\mathrm{Br}(B_s^0 \to \mu^+\mu^-)$, the value corresponds to the value before integration over time, i.e., removing the effect of $\Delta\Gamma_s$. For $\mathrm{Br}(B^0 \to \mu^+\mu^-)$, an upper bound is available, but the statistical significance is too low to quote a measurement in the right-hand column. Modified from the CKMfitter Group (manuscript in preparation).

measurements). Other quantities are still far from being measured as accurately as their prediction from the global fit. Their measurements can help further constrain the CKM parameters, and they still leave room for unexpected deviations from the SM picture emerging from the global fit.

4.2. Analyses of Deviations from the CKM Paradigm

Quark flavor physics provides both stringent tests of the SM and significant constraints on NP models. However, the above-described processes used to determine the CKM parameters show good overall consistency within the SM, and thus lead to upper bounds on additional NP contributions. Additional processes suffering from larger theoretical or experimental uncertainties must therefore be included in the global analyses in order to probe physics beyond the SM.

Although specific NP models could be directly compared with experimental results, it is natural to consider effective approaches for flavor processes. The short-distance dynamics is encoded in Wilson coefficients multiplied by operators describing the transition on long distances (24), given that these flavor processes take place at significantly lower energies than the NP degrees of freedom of interest. NP affects the values of the Wilson coefficients. The structure of the operators affected (e.g., vector, scalar) provides a hint of the type of NP at play, and the deviations of the Wilson coefficients from SM expectations provide an idea of the energy scales and coupling constants involved. In any case (specific NP models or general effective approaches), the above constraints must be reconsidered in order to learn whether they can be used to determine CKM parameters, constrain NP contributions, or neither.

We discuss two topical examples in the following subsections. The first is NP arising in $\Delta F = 2$ processes, and the second is NP violating lepton flavor universality in $\Delta F = 1$ processes.

4.2.1. New Physics in $\Delta F = 2$. As discussed elsewhere (77, 183, 231–238) and in Section 3.4.1, neutral-meson mixing is a particularly interesting probe of NP. The evolution of the $B_q \bar{B}_q$ system is described through a quantum-mechanical Hamiltonian $H = M^q - i\Gamma^q/2$ as the sum of two Hermitian "mass" and "decay" matrices, so that $B^0_{(s)}$–$\overline{B}^0_{(s)}$ oscillations involve the off-diagonal elements M^q_{12} and Γ^q_{12}, respectively. The three physical quantities $|M^q_{12}|$, $|\Gamma^q_{12}|$, and $\varphi_q = \arg(-M^q_{12}/\Gamma^q_{12})$ can be determined from the mass difference $\Delta m_q \simeq 2|M^q_{12}|$ among the eigenstates, their width difference $\Delta\Gamma_q \simeq 2\,|\Gamma^q_{12}|\cos\varphi_q$, and the semileptonic CP asymmetry $a^q_{\mathrm{SL}} = \mathrm{Im}\Gamma^q_{12}/M^q_{12} = \Delta\Gamma_q/\Delta m_q \tan\varphi_q$. Resulting from box diagrams with heavy (virtual) particles, M^q_{12} is expected to be especially sensitive to NP (77), so that the two complex parameters Δ_s and Δ_d, defined as

$$M^q_{12} \equiv M^{\mathrm{SM},q}_{12}\,\Delta_q, \quad \Delta_q \equiv |\Delta_q| e^{i\varphi^\Delta_q}, \quad q = d, s, \tag{19.}$$

can differ substantially from the SM value $\Delta_s = \Delta_d = 1$.

Importantly, the NP phases $\varphi^\Delta_{d,s}$ not only affect $a^{d,s}_{\mathrm{SL}}$ but also shift the CP phases extracted from the mixing-induced CP asymmetries in $B^0 \to J/\psi\, K^0_S$ and $B^0_s \to J/\psi\, \phi$ to $2\beta + \varphi^\Delta_d$ and $2\beta_s - \varphi^\Delta_s$, respectively. If it is assumed that NP enters only through the two parameters Δ_d and Δ_s, the CKM paradigm is still valid to analyze $\Delta F = 1$ quark flavor transitions. By contrast, the $\Delta F = 2$ transitions previously used to determine the CKM parameters must be reinterpreted as constraints on Δ_d and Δ_s [namely Δm_d, Δm_s, $\sin(2\beta)$ and α].

There has been a great deal of interest in such NP scenarios triggered by deviations observed first in early measurements from CDF and D0 on the B^0_s mixing angle φ_s, and later after D0 quoted values of the like-sign dimuon asymmetry a_{SL} (measuring a linear combination of a^d_{SL} and a^s_{SL}). However, as discussed in Section 3.4.1, later measurements of the individual semileptonic CP asymmetries and mixing angles for B^0 and B^0_s mesons have not been able to explain the D0 measurement, as they showed good agreement with SM expectations.

Simultaneous fits of the CKM parameters and the NP parameters Δ_d and Δ_s have been performed (77, 183) in different generic scenarios in which NP is confined to $\Delta F = 2$ flavor-changing neutral currents. The most recent update (93) used data up to summer 2014. The two complex NP parameters Δ_d and Δ_s are not sufficient to absorb the discrepancy between the D0 measurement of a_{SL} and the rest of the global fit (93). Without a_{SL}, the fit including NP in $\Delta F = 2$ is good, but the improvement with respect to the SM is limited. In the case of the so-called scenario I (Δ_s and Δ_d independent), the following values are obtained:

$$\Delta_d = (0.94^{+0.18}_{-0.15}) + i(-0.12^{+0.12}_{-0.05}) \qquad \Delta_s = (1.05^{+0.14}_{-0.13}) + i(0.03^{+0.04}_{-0.04}), \tag{20.}$$

together with the following values of the CKM parameters:

$$A = 0.790^{+0.038}_{-0.008}, \quad \lambda = 0.2258^{+0.0005}_{-0.0006}, \quad \bar{\rho} = 0.136^{+0.022}_{-0.028}, \quad \bar{\eta} = 0.402^{+0.015}_{-0.054}. \tag{21.}$$

The constraints are shown in **Figure 8**. The data still allow sizable NP contributions in both B^0 and B^0_s sectors up to 30–40% at the 3σ level. The results for the CKM parameters can be compared with those of Equation 16, with the caveat that the inputs are different. Unsurprisingly,

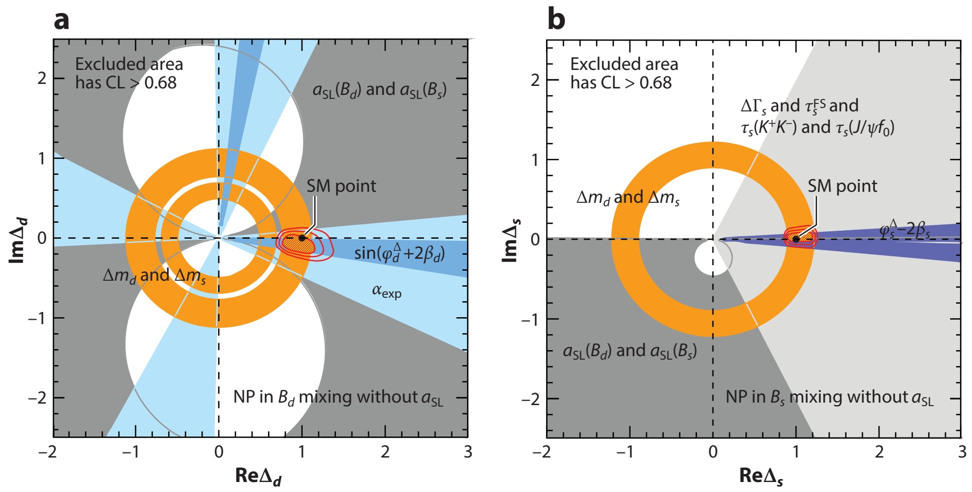

Figure 8

Complex parameters (*a*) Δ_d and (*b*) Δ_s describing New Physics (NP) in $\Delta F = 2$ (Scenario I, not including a_{SL}). The colored areas represent regions with $1 - p < 68.3\%$ for the individual constraints. The red area represents the region with $1 - p < 68.3$ % for the combined fit, with the two additional contours delimiting the regions with $1 - p < 95.45$ % and $1 - p < 99.73$ %. Abbreviation: SM, Standard Model. Modified from Reference 93.

there is a wider range of variations of the CKM parameters once some of the constraints involve not only SM but also NP contributions.

The same kind of analysis has also been used for prospective studies that take into account the accuracies expected from the full data sets of the LHCb phase 1 upgrade and Belle-II (238). Assuming no signal of NP, the constraints on Δ_d and Δ_s tighten, setting stringent constraints on the scale of NP involved, which can range from 10 to 10^3 TeV, depending on the structure of couplings chosen.

4.2.2. Violation of lepton flavor universality in $\Delta F = 1$ processes. As discussed in Section 3.5, there are interesting hints of a breakdown of lepton flavor universality in both $b \to c\ell\nu$ and $b \to s\ell\ell$ processes. Both types of processes have been analyzed to extract information about potential NP contributions in the effective Hamiltonian approach describing the process at the scale $\mu_b = O(m_b)$ around the b quark mass after integrating out heavier degrees of freedom (24).

For the $b \to c\ell\nu$ transitions, the ratios of the branching ratios $R(D)$ and $R(D^*)$ do not involve CKM parameters. The deviations can be easily interpreted by adding new interactions to the effective Hamiltonian, for instance, additional NP scalar couplings (239). A more extensive study (240) highlights a few scenarios that are compatible not only with the branching ratios but also with the q^2 shape of the $B \to D\tau\bar{\nu}_\tau$ differential decay rate. Two-dimensional scenarios with left- and right-handed couplings, either vector or scalar, are favored. Note that the $B \to D\ell\bar{\nu}_\ell$ form factors are known from lattice QCD simulations (241, 242), but this is not the case for the $B \to D^*\ell\bar{\nu}_\ell$ decay, whose prediction requires many additional theoretical assumptions (validity of heavy-quark effective theory, absence of NP for electrons and muons). Moreover, presently there are only a very limited number of observables (two ratios of branching ratios). The geometry of the decay products could add further information about the deviations observed in the branching ratios (243) and could enable one to check the q^2 dependence of the differential decay rates for both vector and pseudoscalar final mesons.

There is a much larger set of observables concerning $b \to s\ell^+\ell^-$ decays, with many different channels. Interest in a global analysis of such decays was clear long before the advent of B -factory and LHCb data (244). The appearance of several tensions in different $b \to s\ell^+\ell^-$ channels is interesting because all these observables are sensitive to the same couplings $\mathcal{C}^{(\prime)}_{7,9,10}$ induced by the local four-fermion operators in the effective Hamiltonian approach:

$$\mathcal{O}^{(\prime)}_9 = \frac{\alpha}{4\pi}[\bar{s}\gamma^\mu P_{L(R)}b][\bar{\mu}\gamma_\mu\mu], \qquad \mathcal{C}^{\mathrm{SM}}_9(\mu_b) = 4.07, \tag{22}$$
$$\mathcal{O}^{(\prime)}_{10} = \frac{\alpha}{4\pi}[\bar{s}\gamma^\mu P_{L(R)}b][\bar{\mu}\gamma_\mu\gamma_5\mu], \quad \mathcal{C}^{\mathrm{SM}}_{10}(\mu_b) = -4.31,$$
$$\mathcal{O}^{(\prime)}_7 = \frac{\alpha}{4\pi}m_b[\bar{s}\sigma_{\mu\nu}P_{R(L)}b]F^{\mu\nu}, \qquad \mathcal{C}^{\mathrm{SM}}_7(\mu_b) = -0.29,$$

where $P_{L,R}$ project on left- and right-handed chiralities and primed operators have vanishing or negligible Wilson coefficients $\mathcal{C}'_{7,9,10}$ in the SM. The couplings $\mathcal{C}^{(\prime)}_{7,9,10}$ can be constrained through various observables in radiative and (semi-)leptonic $B^0_{(s)}$ decays, each of them sensitive to different subsets and combinations of coefficients. The first analyses performed in this spirit and exploiting LHCb data (245) pointed to a large contribution to the Wilson coefficient $\mathcal{C}_9$ in $b \to s\mu^+\mu^-$, which was quickly confirmed (246, 247). Three recent global analyses (248–250) have been performed, involving similar sets of data. There are also several analyses that have included the latest observables violating lepton-flavor universality such as R_{K^*} (251–256). They rely on different inputs and hypotheses but agree in their conclusions and prefer scenarios involving a significant contribution to $\mathcal{C}_9(m_b) \simeq -1.1$ in $b \to s\mu^+\mu^-$, whereas contributions to other Wilson coefficients are only loosely bound and compatible with the SM. Intense theoretical activity is currently under way to cross-check the various sources of theoretical uncertainties [power corrections to the limit $m_b \to \infty$, form factors, long-distance charm-loop contributions (257–261a)], confirming the robustness of this picture up to now.

As there is no clear picture for NP models that could be responsible for the deviations in both $b \to c\ell\nu$ and $b \to s\ell^+\ell^-$ decays (even though leptoquarks, Z' bosons, and partial compositeness models are favored), it is not easy to perform a combined fit of the CKM parameters and NP contributions in a way similar to the $\Delta F = 2$ case reported in Section 4.2.1. Indeed, the NP analyses have often assumed values of the CKM parameters based either on full global fits or on tree-level determinations, assuming that the uncertainty coming from the CKM parameters is subleading compared with other sources of uncertainties.

However, if there is a violation of lepton flavor universality, all leptonic and semileptonic decays may be significantly affected. Unfortunately, not all measurements are given for muonic and electronic modes separately. Removing all these modes from the determination of the CKM parameters leads to

$$A = 0.831^{+0.058}_{-0.109}, \quad \lambda = 0.213^{+0.010}_{-0.005}, \quad \bar{\rho} = 0.127^{+0.019}_{-0.019}, \quad \bar{\eta} = 0.350^{+0.012}_{-0.011}, \tag{23}$$
$$|V_{cb}| = 0.0421^{+0.0011}_{-0.0016}, \quad |V_{ts}| = 0.0414^{+0.0010}_{-0.0016}.$$

A second approach is also possible, following the current experimental indications that electron modes are in agreement with SM. Only the μ and τ modes should be removed from the global fit to the CKM parameters, leading to

$$A = 0.831^{+0.021}_{-0.031}, \quad \lambda = 0.2251^{+0.0004}_{-0.0004}, \quad \bar{\rho} = 0.155^{+0.008}_{-0.008}, \quad \bar{\eta} = 0.340^{+0.010}_{-0.010}, \tag{24}$$
$$|V_{cb}| = 0.0425^{+0.0007}_{-0.0018}, \quad |V_{ts}| = 0.0410^{+0.0014}_{-0.0012}.$$

In both cases, $|V_{tb}|$ is unity up to a very high accuracy. These results can be compared with those from the SM global fit in Equation 16:

$$|V_{cb}| = 0.0418^{+0.0003}_{-0.0006}, \quad |V_{ts}| = 0.0411^{+0.0003}_{-0.0006}. \qquad 25.$$

Removing part or all the modes potentially affected by the violation of lepton flavor universality significantly increases the uncertainties (up to a factor of five) on the CKM matrix elements $|V_{cb}|$ and $|V_{ts}|$, which arise in $b \to c\ell\nu$ and $b \to s\ell\ell$ decays, respectively. However, considering the other experimental and theoretical uncertainties involved, the parametric uncertainty coming from CKM parameters indeed remains subleading for the NP analyses of these modes, and it should not alter their conclusions.

5. OUTLOOK

The CKM matrix is a key element in the description of flavor dynamics in the SM. With only four parameters, this matrix is able to describe a wide range of phenomena, such as *CP* violation and rare decays. It can thus be constrained by many different processes, which have to be measured experimentally with high accuracy and computed with good theoretical control. After the first LEP measurements, the turn of the millennium has opened the B-factory era, leading to a remarkable improvement in the number and accuracy of the constraints set on the CKM matrix, which exhibit remarkable consistency and have led to a precise determination of the CKM parameters.

The status presented in Section 3 is based on experiments up to and including the lifetime of the B factories, as well as LHC Run 1. The corresponding data sets have been almost fully exploited, whereas no updated measurements using data from the ongoing Run 2 are yet available. This situation will soon change, as the first Run 2 analyses will shortly be released by LHCb, ATLAS, and CMS. A change of gear is expected after the year 2020, when both Belle-II and the phase 1 upgraded LHCb experiment will collect data at much higher luminosities. The target is a multiplication of the data sets by up to two orders of magnitude (262, 263). In the case of LHCb, this includes the increase of the $b\bar{b}$ cross section at higher energies and an improved trigger (264). A reduction of experimental uncertainties by factors of around 10 on the angles β, γ, and φ_s is to be expected, as no irreducible systematic uncertainties are foreseen to affect the results in the foreseeable future. One may also expect improvements in the experimental measurements of the observables related to the angle α and the matrix elements $|V_{ub}|$ and $V|_{cb}$. In addition, new measurements concerning lepton flavor universality and observables in rare decays are likely to be presented in the coming years.

The interpretation of these improved measurements will depend on developments in theoretical calculations. The computation using lattice QCD simulations has already reached a very mature stage for some of the quantities described in Section 4, for instance, decay constants and form factors. At the accuracy obtained, some issues become relevant, such as the estimation of electromagnetic corrections, the detailed extrapolation in heavy-quark masses, and the kinematic range available for heavy to light form factors. Hopefully, the resulting improvement in the accuracy of the theoretical computations will resolve the puzzles currently affecting the determination of $|V_{ub}|$ and $|V_{cb}|$. More generally, the experimental accuracy obtained for the individual constraints requires one to reassess some of the theoretical hypotheses commonly used to extract these quantities and add systematics that have been neglected up to now (e.g., sources of isospin breaking arising in the determination of α, penguin pollution for β). Other improvements can be expected concerning more exploratory domains, such as the matrix elements of operators beyond the SM (which are needed to analyze flavor constraints in NP models) or quantities involving hadrons difficult to access up to now—for instance, unstable mesons decaying under the strong interaction (e.g., ρ, K^*) or light or heavy baryons (e.g., nucleons, hyperons, Λ_b). Progress can also be expected from other theoretical methods (e.g., effective theories, dispersive approaches). Even though it is more difficult to assess their impact on the study of the CKM matrix, these advances should help in the study of ϵ'/ϵ, the constraints on NP from neutral-meson mixing, or the interpretation of anomalies in rare b decays.

The current picture provided by global fits to CKM parameters within the SM is both accurate and consistent, and it shows that this approach can be used to study NP models affecting flavor dynamics (such as models with NP in $\Delta F = 2$ transitions). Such analyses extend the initial objective of constraining the CKM matrix, and they require a joint determination of the CKM parameters and NP contributions, based on a larger set of measured observables. Such analyses extend the initial objective of constraining the CKM matrix, and they require a joint determination of the CKM parameters and NP contributions. This approach through global fits is currently relevant for the study of hints of violation of lepton flavor universality in $b \to c$ and $b \to s$ transitions, which have sparked a great deal of interest. Several attempts to analyze these deviations in terms of model-independent effective approaches exist, but these results still need to be connected with viable high-energy models. In these challenging analyses, the uncertainties related to CKM parameters are subleading compared with other (experimental and hadronic) uncertainties. A consistent picture of whether lepton universality holds may become available soon, which could provide original directions for these studies.

More generally, new developments in flavor physics can be expected through the improved determination of CKM parameters, the identification of departures from the SM in flavor transitions, and the study of heavy degrees of freedom through low-energy processes at high intensity. In all of these areas, upcoming measurements from LHCb and Belle-II and ongoing progress in theoretical computations will play an essential role in the near future.

DISCLOSURE STATEMENT

The authors are not aware of any affiliations, memberships, funding, or financial holdings that might be perceived as affecting the objectivity of this review.

ACKNOWLEDGMENTS

S.D.G. thanks his collaborators from the CKMfitter Group for discussions and comments on many issues covered in this review. S.D.G. acknowledges partial support from contract FPA2014-61478-EXP. This work has received funding from the European Union's Horizon 2020 research and innovation program under grant agreements 690575, 674896, and 692194. This work is also part of the NWO Institute Organisation (NWO-I), which is financed by the Netherlands Organisation for Scientific Research (NWO).

LITERATURE CITED

1. Aad G, et al. *Phys. Lett. B* 716:1 (2012)
2. Chatrchyan S, et al. *Phys. Lett. B* 716:30 (2012)
3. Cabibbo N. *Phys. Rev. Lett.* 10:531 (1963)
4. Kobayashi M, Maskawa T. *Prog. Theor. Phys.* 49:652 (1973)
5. Sakharov AD. *Pisma Zh. Eksp. Teor. Fiz.* 5:32 (1967)
6. Cohen AG, Kaplan D, Nelson A. *Annu. Rev. Nucl. Part. Sci.* 43:27 (1993)
7. Riotto A, Trodden M. *Annu. Rev. Nucl. Part. Sci.* 49:35 (1999)
8. Hou WS. *Chin. J. Phys.* 47:134 (2009)

9. Wolfenstein L. *Phys. Rev. Lett.* 51:1945 (1983)
10. Jarlskog C. *Phys. Rev. Lett.* 55:1039 (1985)
11. Jeitler M. *Nucl. Instrum. Methods A* 478:404 (2002)
12. Aloisio A, et al. *The KLOE detector: technical proposal.* Report LNF-93-002-IR, Frascati, Italy (1993)
13. Amelino-Camelia G, et al. *Eur. Phys. J. C* 68:619 (2010)
14. Albrecht H, et al. *Nucl. Instrum. Methods A* 275:1 (1989)
15. Andrews D, et al. *Nucl. Instrum. Methods* 211:47 (1983)
16. Aubert B, et al. *Nucl. Instrum. Methods A* 479:1 (2002)
17. Abashian A, et al. *Nucl. Instrum. Methods A* 479:117 (2002)
18. Kuhr T. *Springer Tracts Mod. Phys.* 249:1 (2013)
19. Abe T, et al. arXiv:1011.0352 [physics.ins-det] (2010)
20. Alves AA Jr., et al. *J. Instrum.* 3:S08005 (2008)
21. Aad G, et al. *J. Instrum.* 3:S08003 (2008)
22. Chatrchyan S, et al. *J. Instrum.* 3:S08004 (2008)
23. Ablikim M, et al. *Nucl. Instrum. Methods A* 614:345 (2010)
24. Buchalla G, Buras AJ, Lautenbacher ME. *Rev. Mod. Phys.* 68:1125 (1996)
25. Patrignani C, et al. *Chin. Phys. C* 40:100001 (2016)
26. Aoki S, et al. *Eur. Phys. J. C* 77:112 (2017)
27. Antonelli M, et al. *Eur. Phys. J. C* 69:399 (2010)
28. Ablikim M, et al. *Phys. Rev. D* 89:051104 (2014)
29. Zupanc A, et al. *J. High Energy Phys.* 09:139 (2013)
30. Alexander JP, et al. *Phys. Rev. D* 79:052001 (2009)
31. del Amo Sanchez P, et al. *Phys. Rev. D* 82:091103 (2010); del Amo Sanchez P, et al. Erratum. *Phys. Rev. D* 91:019901 (2015)
32. Onyisi PUE, et al. *Phys. Rev. D* 79:052002 (2009)
33. Naik P, et al. *Phys. Rev. D* 80:112004 (2009)
34. Ablikim M, et al. *Phys. Rev. D* 92:072012 (2015)
35. Lees JP, et al. *Phys. Rev. D* 91:052022 (2015)
36. Besson D, et al. *Phys. Rev. D* 80:032005 (2009)
37. Widhalm L, et al. *Phys. Rev. Lett.* 97:061804 (2006)
38. Aubert B, et al. *Phys. Rev. D* 76:052005 (2007)
39. Burdman G, Goldman JT, Wyler D. *Phys. Rev. D* 51:111 (1995)
40. Becirevic D, Haas B, Kou E. *Phys. Lett. B* 681:257 (2009)
41. Hardy JC, Towner IS. *Phys. Rev. C* 91:025501 (2015)
42. Amhis Y, et al. arXiv:1412.7515 [hep-ex] (updated results and plots available at **http://www.slac.stanford.edu/xorg/hfag/**) (2014)
43. Aubert B, et al. *Phys. Rev. D* 79:012002 (2009)
44. Dungel W, et al. *Phys. Rev. D* 82:112007 (2010)
45. Aubert B, et al. *Phys. Rev. Lett.* 104:011802 (2010)
46. Urquijo P, et al. *Phys. Rev. D* 75:032001 (2007)
47. Schwanda C, et al. *Phys. Rev. D* 75:032005 (2007)
48. Aubert B, et al. *Phys. Rev. D* 69:111104 (2004)
49. Aubert B, et al. *Phys. Rev. D* 81:032003 (2010)
50. Shifman MA, Vainshtein AI, Zakharov VI. *Nucl. Phys. B* 147:385 (1978)
51. Shifman MA, Vainshtein AI, Zakharov VI. *Nucl. Phys. B* 147:448 (1978)
52. Alberti A, Gambino P, Healey KJ, Nandi S. *Phys. Rev. Lett.* 114:061802 (2015)
53. Gambino P, Schwanda C. *Phys. Rev. D* 89:014022 (2014)
54. Bailey JA, et al. *Phys. Rev. D* 92:014024 (2015)
55. Flynn JM, et al. *Phys. Rev. D* 91:074510 (2015)
56. Dalgic E, et al. *Phys. Rev. D* 73:074502 (2006); Dalgic E, et al. Erratum. *Phys. Rev. D* 75:119906 (2007)
57. Ha H, et al. *Phys. Rev. D* 83:071101 (2011)
58. Lees JP, et al. *Phys. Rev. D* 86:092004 (2012)
59. del Amo Sanchez P, et al. *Phys. Rev. D* 83:032007 (2011)

60. Lees JP, et al. *Phys. Rev. D* 86:032004 (2012)
61. Aubert B, et al. *Phys. Rev. D* 73:012006 (2006)
62. Aubert B, et al. *Phys. Rev. Lett.* 95:111801 (2005); Aubert B, et al. Erratum. *Phys. Rev. Lett.* 97:019903 (2006)
63. Limosani A, et al. *Phys. Lett. B* 621:28 (2005)
64. Bornheim A, et al. *Phys. Rev. Lett.* 88:231803 (2002)
65. Lange BO, Neubert M, Paz G. *Phys. Rev. D* 72:073006 (2005)
66. Bauer CW, Ligeti Z, Luke ME. *Phys. Rev. D* 64:113004 (2001)
67. Aglietti U, Di Lodovico F, Ferrera G, Ricciardi G. *Eur. Phys. J. C* 59:831 (2009)
68. Gambino P, Giordano P, Ossola G, Uraltsev N. *J. High Energy Phys.* 10:058 (2007)
69. Gardi E. Presented at Rencontres de Physique de la Vallée d'Aoste, 22nd, La Thuile, Italy, Feb. 24–March 1 (2008)
70. Bigi IIY, et al. *Phys. Rev. Lett.* 71:496 (1993)
71. Bigi IIY, et al. *Int. J. Mod. Phys. A* 9:2467 (1994)
72. Schwanda C, et al. *Phys. Rev. D* 78:032016 (2008)
73. Lees JP, et al. *Phys. Rev. D* 88:031102 (2013)
74. Kronenbitter B, et al. *Phys. Rev. D* 92:051102 (2015)
75. Adachi I, et al. *Phys. Rev. Lett.* 110:131801 (2013)
76. Aubert B, et al. *Phys. Rev. D* 81:051101 (2010)
77. Lenz A, et al. *Phys. Rev. D* 83:036004 (2011)
78. Aaij R, et al. *Nat. Phys.* 11:743 (2015)
79. Detmold W, Lehner C, Meinel S. *Phys. Rev. D* 92:034503 (2015)
80. Patrignani C, et al. *Chin. Phys. C* 40:100001 (2016)
81. Lacker H, et al. *Eur. Phys. J. C* 72:2048 (2012)
82. Aubert B, et al. *Phys. Rev. Lett.* 87:091801 (2001)
83. Abe K, et al. *Phys. Rev. Lett.* 87:091802 (2001)
84. Carter AB, Sanda A. *Phys. Rev. D* 23:1567 (1981)
85. Bigi IIY, Sanda AI. *Phys. Rev. D* 29:1393 (1984)
86. Bigi IIY, Sanda AI. *Nucl. Phys. B* 193:85 (1981)
87. Bevan AJ, et al. *Eur. Phys. J. C* 74:3026 (2014)
88. Aubert B, et al. *Phys. Rev. D* 79:072009 (2009)
89. Adachi I, et al. *Phys. Rev. Lett.* 108:171802 (2012)
90. Aaij R, et al. *Phys. Rev. Lett.* 115:031601 (2015)
91. Aubert B, et al. *Phys. Rev. D* 71:032005 (2005)
92. Itoh R, et al. *Phys. Rev. Lett.* 95:091601 (2005)
93. Charles J, et al. *Phys. Rev. D* 91:073007 (2015)
94. De Bruyn K, Fleischer R. *J. High Energy Phys.* 03:145 (2015)
95. De Bruyn K, Fleischer R, Koppenburg P. *Eur. Phys. J. C* 70:1025 (2010)
96. Aubert B, et al. *Phys. Rev. Lett.* 101:021801 (2008)
97. Lee SE, et al. *Phys. Rev. D* 77:071101 (2008)
98. Aaij R, et al. *Phys. Lett. B* 742:38 (2015)
99. Aaij R, et al. *J. High Energy Phys.* 06:131 (2015)
100. Jung M. *Phys. Rev. D* 86:053008 (2012)
101. Frings P, Nierste U, Wiebusch M. *Phys. Rev. Lett.* 115:061802 (2015)
102. Šantelj L, et al. *J. High Energy Phys.* 10:165 (2014)
103. Aubert B, et al. *Phys. Rev. D* 79:052003 (2009)
104. Beneke M. *Phys. Lett. B* 620:143 (2005)
105. Aaij R, et al. *Eur. Phys. J. C* 72:2022 (2012)
106. Aaij R, et al. *J. Instrum.* 10:P10005 (2015)
107. Aaij R, et al. *J. Instrum.* 11:P05010 (2016)
108. Aaij R, et al. *Eur. Phys. J. C* 77:238 (2017)
109. Gronau M, London D. *Phys. Rev. Lett.* 65:3381 (1990)
110. Lipkin HJ, Nir Y, Quinn HR, Snyder A. *Phys. Rev. D* 44:1454 (1991)

111. Lees JP, et al. *Phys. Rev. D* 87:052009 (2013)
112. Adachi I, et al. *Phys. Rev. D* 88:092003 (2013)
113. Aaij R, et al. *J. High Energy Phys.* 10:183 (2013)
114. Bornheim A, et al. *Phys. Rev. D* 68:052002 (2003); Bornheim A, et al. Erratum. *Phys. Rev. D* 75:119907 (2007)
115. Aubert B, et al. *Phys. Rev. D* 76:091102 (2007)
116. Duh YT, et al. *Phys. Rev. D* 87:031103 (2013)
117. Abe K, et al. *Phys. Rev. Lett.* 94:181803 (2005)
118. Aubert B, et al. *Phys. Rev. D* 76:052007 (2007)
119. Vanhoefer P, et al. *Phys. Rev. D* 93:032010 (2016)
120. Aubert B, et al. *Phys. Rev. Lett.* 102:141802 (2009)
121. Zhang J, et al. *Phys. Rev. Lett.* 91:221801 (2003)
122. Aubert B, et al. *Phys. Rev. Lett.* 91:201802 (2003)
123. Kusaka A, et al. *Phys. Rev. D* 77:072001 (2008)
124. Jessop CP, et al. *Phys. Rev. Lett.* 85:2881 (2000)
125. Aubert B, et al. *Phys. Rev. D* 75:091103 (2007)
126. Zhang J, et al. *Phys. Rev. Lett.* 94:031801 (2005)
127. Aubert B, et al. *Phys. Rev. Lett.* 93:051802 (2004)
128. Aubert B, et al. *Phys. Rev. D* 79:072006 (2009)
129. Gronau M, Zupan J. *Phys. Rev. D* 71:074017 (2005)
130. Zupan J. *Nucl. Phys. Proc. Suppl.* 170:33 (2007)
130a. Charles J, Deschamps O, Descotes-Genon S, Niess V. arXiv:1705.02981 [hep-ph] (2017)
131. Brod J, Zupan J. *J. High Energy Phys.* 01:051 (2014)
132. Gronau M, London D. *Phys. Lett. B* 253:483 (1991)
133. Gronau M, Wyler D. *Phys. Lett. B* 265:172 (1991)
134. Atwood D, Dunietz I, Soni A. *Phys. Rev. Lett.* 78:3257 (1997)
135. Atwood D, Dunietz I, Soni A. *Phys. Rev. D* 63:036005 (2001)
136. Giri A, Grossman Y, Soffer A, Zupan J. *Phys. Rev. D* 68:054018 (2003)
137. Insler J, et al. *Phys. Rev. D* 85:092016 (2012); Insler J, et al. Erratum. *Phys. Rev. D* 94:099905 (2016)
138. Malde S, et al. *Phys. Lett. B* 747:9 (2015)
139. Evans T, et al. *Phys. Lett. B* 757:520 (2016)
140. Aaij R, et al. *Phys. Lett. B* 760:117 (2016)
141. Aaij R, et al. *Phys. Rev. D* 91:112014 (2015)
142. Aaij R, et al. *Phys. Rev. D* 92:112005 (2015)
143. Aaij R, et al. *Phys. Rev. D* 93:112018 (2016)
144. Aaij R, et al. *Phys. Lett. B* 733:36 (2014)
145. Aaij R, et al. *J. High Energy Phys.* 10:097 (2014)
146. Aaij R, et al. *J. High Energy Phys.* 08:137 (2016)
147. Aaij R, et al. *J. High Energy Phys.* 11:060 (2014)
148. LHC Collab. Presented at Int. Workshop CKM Unitarity Triangle (CKM 2016), 9th, Mumbai, Nov. 28–Dec. 2. LHCb-CONF-2016-015 (2016)
149. Aaij R, et al. *J. High Energy Phys.* 12:087 (2016)
150. Lees JP, et al. *Phys. Rev. D* 87:052015 (2013)
151. Trabelsi K. Presented at Int. Workshop CKM Unitarity Triangle (CKM 2012), 7th, Cincinnati, Ohio, Sep. 28–Oct. 2 (2012)
152. Aaltonen T, et al. *Phys. Rev. Lett.* 109:171802 (2012)
153. Abazov VM, et al. *Phys. Rev. D* 85:032006 (2012)
154. Khachatryan V, et al. *Phys. Lett. B* 757:97 (2015)
155. Aad G, et al. *J. High Energy Phys.* 08:147 (2016)
156. Aaij R, et al. *Phys. Rev. Lett.* 114:041801 (2015)
157. Aaij R, et al. *Phys. Rev. D* 90:012003 (2014)
158. Aaij R, et al. *Phys. Lett. B* 736:186 (2014)
159. Lenz A, Nierste U. arXiv:1102.4274 [hep-ph] (2011)

160. Lenz A, Nierste U. *J. High Energy Phys.* 06:072 (2007)
161. Charles J, et al. *Eur. Phys. J. C* 41:1 (updated results and plots available at **http://ckmfitter.in2p3.fr**) (2005)
162. Fleischer R. *Eur. Phys. J. C* 10:299 (1999)
163. Fleischer R. *Phys. Rev. D* 60:073008 (1999)
164. Fleischer R. *Nucl. Instrum. Methods A* 446:1 (2000)
165. Faller S, Jung M, Fleischer R, Mannel T. *Phys. Rev. D* 79:014030 (2009)
166. Ciuchini M, Pierini M, Silvestrini L. *Phys. Rev. Lett.* 95:221804 (2005)
167. De Bruyn K. *Searching for penguin footprints: towards high precision* CP *violation measurements in the B meson systems*. PhD thesis, Vrije Univ, Amsterdam, Neth. (2015)
168. Ligeti Z, Robinson DJ. *Phys. Rev. Lett.* 115:251801 (2015)
169. Aaij R, et al. *Nucl. Phys. B* 873:275 (2013)
170. Aaij R, et al. *J. High Energy Phys.* 11:082 (2015)
171. Aaij R, et al. *Phys. Rev. D* 90:052011 (2014)
172. Falk AF, Grossman Y, Ligeti Z, Petrov AA. *Phys. Rev. D* 65:054034 (2002)
173. Nierste U. In *Proceedings of the Helmholtz International School Heavy Quark Physics* (*HQP08*), ed. A Ali, M Ivanov, p. 1. Hamburg, Ger.: DESY (2009)
174. Beneke M, Buchalla G, Dunietz I. *Phys. Rev. D* 54:4419 (1996); Beneke M, Buchalla G, Dunietz I. Erratum. *Phys. Rev. D* 83:119902 (2011)
175. Beneke M, et al. *Phys. Lett. B* 459:631 (1999)
176. Ciuchini M, et al. *J. High Energy Phys.* 08:031 (2003)
177. Bigi IIY, Uraltsev NG, Vainshtein AI. *Phys. Lett. B* 293:430 (1992)
178. De Bruyn K, et al. *Phys. Rev. D* 86:014027 (2012)
179. De Bruyn K, et al. *Phys. Rev. Lett.* 109:041801 (2012)
180. Khachatryan V, et al. *Nature* 522:68 (2015)
181. Aaboud M, et al. *Eur. Phys. J. C* 76:513 (2016)
182. Beneke M, et al. *Nucl. Phys. B* 639:389 (2002)
183. Lenz A, et al. *Phys. Rev. D* 86:033008 (2012)
184. Abazov VM, et al. *Phys. Rev. D* 89:012002 (2014)
185. Lees JP, et al. *Phys. Rev. Lett.* 114:081801 (2015)
186. Lees JP, et al. *Phys. Rev. Lett.* 111:101802 (2013); Lees JP, et al. Addendum. *Phys. Rev. Lett.* 111:159901 (2013)
187. Nakano E, et al. *Phys. Rev. D* 73:112002 (2006)
188. Abazov VM, et al. *Phys. Rev. Lett.* 110:011801 (2013)
189. Abazov VM, et al. *Phys. Rev. D* 86:072009 (2012)
190. Aaij R, et al. *Phys. Rev. Lett.* 114:041601 (2015)
191. Aaij R, et al. *Phys. Rev. Lett.* 117:061803 (2016)
192. Borissov G, Hoeneisen B. *Phys. Rev. D* 87:074020 (2013)
193. Buras AJ, Jamin M, Weisz PH. *Nucl. Phys. B* 347:491 (1990)
194. Brod J, Gorbahn M. *Phys. Rev. D* 82:094026 (2010)
195. Brod J, Gorbahn M. *Phys. Rev. Lett.* 108:121801 (2012)
196. Batley JR, et al. *Phys. Lett. B* 544:97 (2002)
197. Abouzaid E, et al. *Phys. Rev. D* 83:092001 (2011)
198. Bai Z, et al. *Phys. Rev. Lett.* 115:212001 (2015)
199. Buras AJ. *J. High Energy Phys.* 04:071 (2016)
200. Buras AJ, Gérard JM. *J. High Energy Phys.* 12:008 (2015)
201. Kitahara T, Nierste U, Tremper P. *J. High Energy Phys.* 12:078 (2016)
202. Blake T, Gershon T, Hiller G. *Annu. Rev. Nucl. Part. Sci.* 65:113 (2015)
203. Aaij R, et al. *Phys. Rev. Lett.* 113:151601 (2014)
204. Lees JP, et al. *Phys. Rev. Lett.* 109:101802 (2012)
205. Lees JP, et al. *Phys. Rev. D* 88:072012 (2013)
206. Huschle M, et al. *Phys. Rev. D* 92:072014 (2015)
207. Abdesselam A, et al. arXiv:1603.06711 [hep-ex] (2016)

208. Aaij R, et al. *Phys. Rev. Lett.* 115:111803 (2015)
209. Hirose S, et al. *Phys. Rev. Lett.* 118:211801 (2017)
210. LHCb Collab. Test of lepton universality with $B^0 \rightarrow K^{*0}\ell + \ell^-$ decays. Report LHCb-PAPER-2017-013, Geneva (2017)
211. Aaij R, et al. *J. High Energy Phys.* 02:104 (2016)
212. Descotes-Genon S, Matias J, Ramon M, Virto J. *J. High Energy Phys.* 01:048 (2013)
213. Sato Y, et al. *Phys. Rev. D* 94:072007 (2016)
214. Wehle S, et al. *Phys. Rev. Lett.* 118:111801 (2017)
215. Aaij R, et al. *J. High Energy Phys.* 07:084 (2013)
216. Aaij R, et al. *J. High Energy Phys.* 06:133 (2014)
217. Aaij R, et al. *J. High Energy Phys.* 06:115 (2015)
218. Aaij R, et al. *J. High Energy Phys.* 09:179 (2015)
219. Battaglia M, et al. arXiv:hep-ph/0304132 (2003)
220. Charles J, et al. arXiv:hep-ph/0607246 [hep-ph] (2006)
221. Bona M, et al. *Phys. Rev. D* 76:014015 (2007)
222. Charles J, et al. arXiv:hep-ph/0703073 [hep-ph] (2007)
223. Hocker A, Lacker H, Laplace S, Le Diberder F. *Eur. Phys. J. C* 21:225 (2001)
224. Ciuchini M, et al. *J. High Energy Phys.* 07:013 (2001)
225. Eigen G, Dubois-Felsmann G, Hitlin DG, Porter FC. *Phys. Rev. D* 89:033004 (2014)
226. Charles J, Descotes-Genon S, Niess V, Vale Silva L. *Eur. Phys. J. C* 77:214 (2017)
227. Demortier L, Lyons L. *Everything you always wanted to know about pulls*. Tech. rep. CDF/ANAL/PUBLIC/5776. CDF, Batavia, Ill. (2002)
228. Lunghi E, Soni A. *Phys. Lett. B* 666:162 (2008)
229. Buras AJ, Guadagnoli D. *Phys. Rev. D* 78:033005 (2008)
230. Bazavov A, et al. *Phys. Rev. D* 93:113016 (2016)
231. Soares JM, Wolfenstein L. *Phys. Rev. D* 47:1021 (1993)
232. Goto T, Kitazawa N, Okada Y, Tanaka M. *Phys. Rev. D* 53:6662 (1996)
233. Silva JP, Wolfenstein L. *Phys. Rev. D* 55:5331 (1997)
234. Grossman Y, Nir Y, Worah MP. *Phys. Lett. B* 407:307 (1997)
235. Bona M, et al. *J. High Energy Phys.* 03:080 (2006)
236. Ligeti Z, Papucci M, Perez G. *Phys. Rev. Lett.* 97:101801 (2006)
237. Bona M, et al. *J. High Energy Phys.* 03:049 (2008)
238. Charles J, et al. *Phys. Rev. D* 89:033016 (2014)
239. Fajfer S, Kamenik JF, Nisandzic I. *Phys. Rev. D* 85:094025 (2012)
240. Freytsis M, Ligeti Z, Ruderman JT. *Phys. Rev. D* 92:054018 (2015)
241. Na H, et al. *Phys. Rev. D* 92:054510 (2015); Na H, et al. Erratum. *Phys. Rev. D* 93:119906 (2016)
242. Bailey JA, et al. *Phys. Rev. D* 92:034506 (2015)
243. Becirevic D, Fajfer S, Nisandzic I, Tayduganov A. arXiv:1602.03030 [hep-ph] (2016)
244. Ali A, Giudice GF, Mannel T. *Z. Phys. C* 67:417 (1995)
245. Descotes-Genon S, Matias J, Virto J. *Phys. Rev. D* 88:074002 (2013)
246. Altmannshofer W, Straub DM. *Eur. Phys. J. C* 73:2646 (2013)
247. Beaujean F, Bobeth C, van Dyk D. *Eur. Phys. J. C* 74:2897 (2014)
248. Descotes-Genon S, Hofer L, Matias J, Virto J. *J. High Energy Phys.* 06:092 (2016)
249. Altmannshofer W, Straub DM. *Eur. Phys. J. C* 75:382 (2015)
250. Hurth T, Mahmoudi F, Neshatpour S. *Nucl. Phys. B* 909:737 (2016)
251. Ciuchini M, et al. arXiv:1704.05447 [hep-ph] (2017)
252. Geng L-S, et al. arXiv:1704.05446 [hep-ph] (2017)
253. Hiller G, Nisandzic I. arXiv:1704.05444 [hep-ph] (2017)
254. D'Amico G, et al. arXiv:1704.05438 [hep-ph] (2017)
255. Altmannshofer W, Stangl P, Straub DM. arXiv:1704.05435 [hep-ph] (2017)
256. Capdevila B, et al. arXiv:1704.03540 [hep-ph] (2017)
257. Jäger S, Martin Camalich J. *J. High Energy Phys.* 05:043 (2013)
258. Jäger S, Martin Camalich J. *Phys. Rev. D* 93:014028 (2016)

259. Ciuchini M, et al. *J. High Energy Phys.* 06:116 (2016)
260. Descotes-Genon S, Hofer L, Matias J, Virto J. *J. High Energy Phys.* 12:125 (2014)
261. Ciuchini M, et al. Presented at Int. Conf. High Energy Phys. (ICHEP 2016), 38th, Chicago, Aug. 3–10 (2016)
261a. Bobeth C, Chrzaszcz M, van Dyk D, Virto J. arXiv:1707.07305 [hep-ph] (2017)
262. Aushev T, et al. arXiv:1002.5012 [hep-ex] (2010)
263. LHCb Collab. *Framework TDR for the LHCb upgrade: technical design report*. Report LHCb-TDR-012. CERN, Geneva (2012)
264. LHCb Collab. *LHCb trigger and online technical design report*. Report LHCb-TDR-016. CERN, Geneva (2014)